GeoScienceWorld
Lithosphere
Volume 2025, Number 4, Article ID lithosphere_2025_126, 27 pages
https://doi.org/10.2113/2025/lithosphere_2025_126

Lithosphere

Research Article

Neoproterozoic Gabbro and Diorites of the Tianquan County, Longmenshan Orogenic Belt, SW China: U-Pb Ages, Petrogenesis and Tectonic Settings

Inna Safonova,[1] Xiang Ren,[1] Alexandra Gurova,[2,3] Yabo Li,[1] Alina Perfilova,[1] Yunpeng Dong,[4] Anastasiya Krutikova,[2,3] Olga Turkina,[2] Baoping Gan,[1] Qiuming Pei,[1] and Sergei Krivonogov[1]

[1]*Faculty of Geoscience and Engineering, Southwest Jiaotong University, Chengdu, 611756, China*
[2]*Sobolev Institute of Geology and Mineralogy SB RAS, Novosibirsk, 630090, Russia*
[3]*Novosibirsk State University, Novosibirsk, 630090, Russia*
[4]*State Key Laboratory of Continental Evolution and Early Life, Department of Geology, Northwest University, Xi'an, 710069, China*

Correspondence should be addressed to Xiang Ren; xiang.r@hotmail.com

Received 4 March 2025; Revised 11 August 2025; Accepted 23 September 2025; Published 23 October 2025

Academic Editor: Mahmoud Hassan

Petrological and isotope-geochemical studies of magmatic rocks are a necessary part of most tectonic and metallogenic reconstructions, in particular, in orogenic belts formed at active margins of cratonic blocks that experienced long-term and tectonically complicated evolution. Magmatic complexes exposed at the western margin of the Yangtze Block have been studied by many research groups; however, their petrogenesis and tectonic origins remain not fully understood and debatable that limits the validity of this or that tectonic model. In this paper, we present first U-Pb ages, whole-rock geochemical and Sm-Nd and Hf-in-zircon isotope data from gabbroids and diorites exposed in the Tianquan area of the Longmenshan orogenic belt in an attempt to provide more details on their petrogenesis, mantle sources, and tectonic origin. The rocks are calc-alkaline gabbro, gabbro-diorite, and hornblende diorite. There are several compositionally distinct groups: Group 1 gabbro and diorites, Group 2 gabbros, Group 3 diorites, high-Ti gabbro, and monzo-gabbro. Group 1 gabbro (816 Ma) is less enriched in LREE and has less differentiated heavy REE compared to Group 2 gabbros, monzo-gabbro (796 Ma), and high-Ti gabbro (790 Ma). All rocks are characterized by positive εNd(t) and εHf(t). Group 1 gabbros and high-Ti gabbro were derived by high-degree partial melting of depleted harzburgite and spinel lherzolite with participation of subduction-related fluids. Group 1 gabbros experienced 10%–80% fractionation of olivine and clinopyroxene to produce Group 1 diorites (813 and 804 Ma). Group 2 gabbros were derived by low-degree melting of an enriched mantle source affected by slab-derived melts. Group 3 diorites (808 Ma) formed with involvement of subducted sediments. The monzo-gabbro is similar to OIB and formed by a low-degree melted garnet lherzolite. Our data confirm the continuous Neoproterozoic magmatism in western Yangtze. The 860–800 Ma stage of supra-subduction magmatism was followed by a stage of back-arc rifting at ca. 796 Ma.

1. INTRODUCTION

The petrogenesis, mantle sources, and tectonic nature of magmatic rocks composing orogenic belts worldwide represent a necessary basis of tectonic reconstructions and metallogenic prognoses. Intracontinental orogenic belts once formed at active margins in a wide sense (intra-oceanic and continental) of ancient cratonic blocks and/or during oceanic suturing and closure typically include magmatic complexes of various origins: oceanic, supra-subduction, rifting-related, and so on. The tectonic juxtaposition of such complexes in orogenic belts disturbs or hides

their initial relationships and, therefore, impedes robust evaluation of the timing and tectonic settings of their emplacement. In addition to the high-precision geochronological dating, which is indeed of crucial importance for tectonic modeling, petrological and isotope-geochemical studies of magmatic rocks also represent a necessary part of tectonic and metallogenic reconstructions. Such studies help to understand better the conditions of derivation of parental magmas (depth, temperature, degree of partial melting) and their further evolution (fractional crystallization, contamination, mixing, assimilation). Understanding the details of the petrogenesis of magmatic rocks hosted by orogenic belts is necessary for reconstructing both tectonic settings and lithospheric structures. The conditions of petrogenesis are of particular value for orogenic belts that experienced long-term and tectonically complicated evolution.

The orogenic belts surrounding the South China Craton (SCC), in particular, the Yangtze continental block (Figure 1(a)), which formed by Neoproterozoic to early Paleozoic collisions between South China, North China, Australia, India, and Indochina [1–4]. These belts often include magmatic complexes formed in ancient oceanic realms once separating those continents or emplaced at their active margins, in continental or intra-oceanic arc or extensional settings. The northern, northwestern, and western margins of the Yangtze Block are composed of numerous mafic to granitic plutonic rocks and, to a lesser extent, volcanogenic-sedimentary units [5–11].

The western margin of the Yangtze Block is extended from Hannan in the north to Panzhihua in the south and is characterized by a large amount of discontinuous outcrops of Neoproterozoic plutonic complexes and volcano-sedimentary sequences (Figure 1(a)). Some researchers call those complexes a Panxi-Hannan arc [8, 11]. During the past two decades, those intrusions of gabbroids to granitoids have been studied by several research teams, which obtained a large amount of geochronological data indicating their emplacement during a period from 890 to 740 Ma and related tectonic models [e.g. 2, 7, 9, 12–15]. The review made by Zhao et al. advocates that the Neoproterozoic magmatic complexes formed in subduction- and rift-related tectonic settings [11]. However, the northwestern margin of the Yangtze Block remains less studied compared to the northern and western ones, and therefore, the origin and tectonic settings of its hosted magmatic complexes remain not fully understood.

The Tianquan County, our study area, geologically belongs to the Longmenshan orogenic belt, which is located at the northwestern margin of the Yangtze Block separating it from the Songpan-Ganze turbidite basin (Figures 1(a) and 1(b)). Although the main thrust structure of the Longmenshan Belt was formed in Mesozoic time [16, 17], its basement is dominated by Neoproterozoic compositionally mafic to intermediate magmatic complexes [8, 18, 19]. We performed a detailed study of their relationships in the field, the timing of their emplacement (U-Pb zircon ages), petrography, whole-rock geochemistry (major oxides and trace elements), and isotopes (whole-rock Sm-Nd and Hf-in-zircon systematics) in order to identify the age and nature of magmatic complexes, to define mantle sources and track crystallization paths of their parental magmas and, finally, to understand their relationships in space and time in terms of both, petrology and tectonics.

2. GEOLOGICAL SETTING

The study area is located in the Tianquan County, Ya'an City, Sichuan Province, at the junction zone between the western part of the Sichuan Basin and the Songpan-Ganze basin, close to the NE-striking Xianshuihe fault extended along the eastern margin of the Tibetan Plateau and the southwestern Longmenshan orogenic belt (Figure 1). The Longmenshan orogenic belt is extended along the northwestern margin of the Yangtze Block (Figures 1(a) and 1(b)), which is a major part of the SCC. The SCC is bounded by the Qinling-Dabie orogenic belt to the north, Longmenshan orogenic belt from the northwest, and Ailaoshan-Songma suture from the southwest. In the east, the SCC meets the Pacific Plate. The Qinling-Dabie and Longmenshan orogenic belts separate the SCC from the North China Craton and Songpan-Ganze turbidite basin, respectively. The Ailaoshan-Songma suture separates the SCC from the Indochina Block (Figure 1(a)). The SCC formed by the amalgamation of the Yangtze and Cathaysia blocks, but no consensus has been achieved yet on the nature of the Neoproterozoic orogenic belts surrounding the craton due to the variety of magmatic rocks exposed therein [e.g. 3, 11, 20–22]. The basement of the Yangtze Block is dominated by Neoproterozoic formations with a limited portion of Archean to Paleoproterozoic rocks, all covered by Mesozoic strata. The Archean magmatic complexes include tonalitic–trondhjemitic–granodioritic gneisses with subordinate amphibolites and metasedimentary rocks [e.g. 11, 14, 23]. The Paleoproterozoic-Mesoproterozoic units are dominated by sedimentary rocks interlayered with volcanic rocks of Dahongshan, Dongchuan, Hekou, and Kunyang groups in the SW Yangtze Block [24].

The Neoproterozoic rock units of the western Yangtze margin consist of mafic to intermediate volcanic and plutonic rocks, volcaniclastic and sedimentary rocks discontinuously exposed along the western Yangtze Block and extend from the Hannan region in the north to the Panzhihua region in the south (Figure 1(a)). The plutonic granitoids form large batholiths, and the mafic to diorite rocks occur as numerous stocks (medium to small size plutons) and dykes [e.g. 15, 25–28]. The volcano-sedimentary rocks belong to the Yanbian and Bikou groups and Suxiong Formation. The Yanbian Group is exposed in the southwestern Yangtze Block and comprises thick basaltic lava flows in the lower part and flysch deposits in the upper part [10, 29]. Detrital zircon ages of sandstones yielded a maximum depositional age of ca. 870 Ma [30]. The Bikou Group is exposed in the northwestern Yangtze Block and consists of greenschist-facies metamorphosed volcanic rocks, volcaniclastic rocks, and clastic sedimentary rocks of ca. 845–775 Ma in age [e.g. 31–34]. The Suxiong Formation is exposed in the middle part of the western

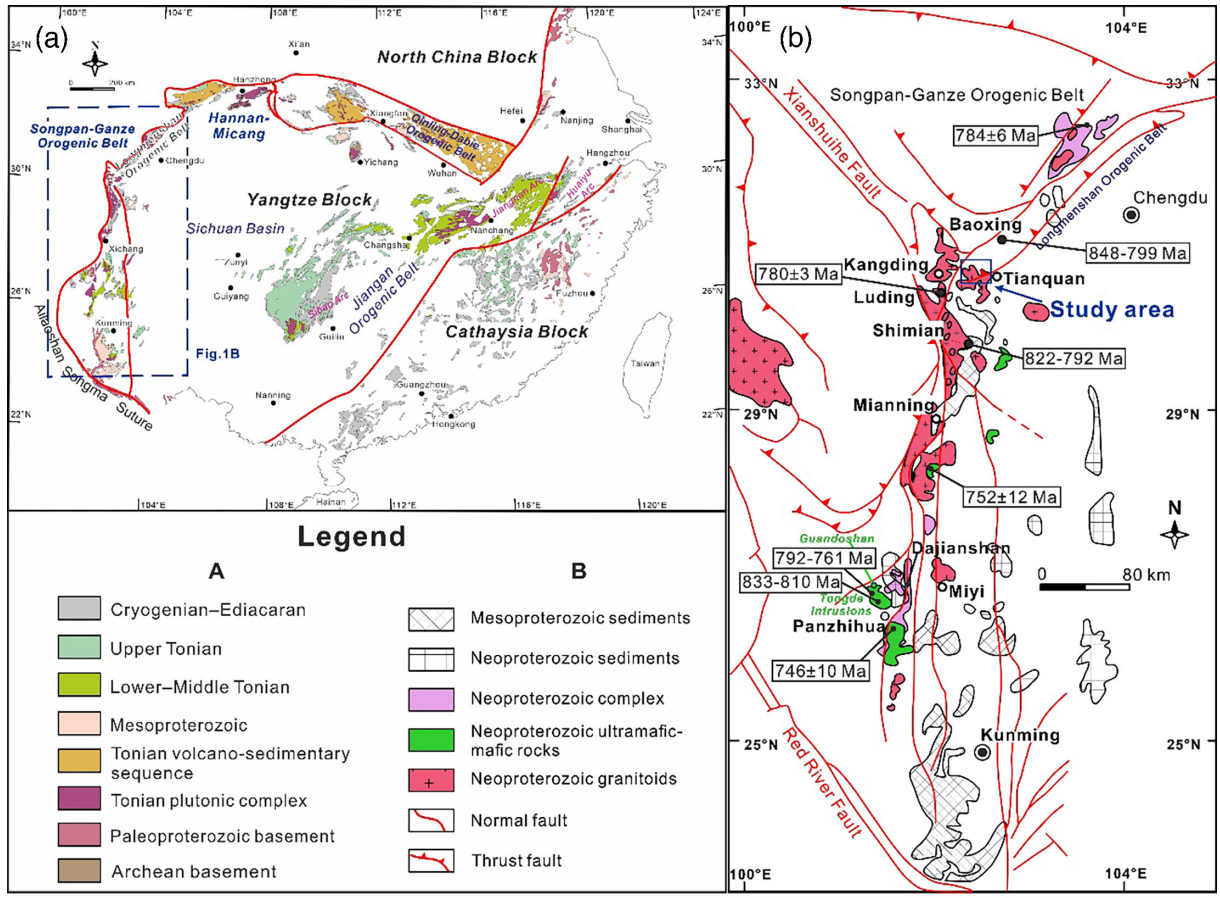

FIGURE 1: (a) Schematic geological map of the South China Craton showing the distribution of Precambrian rocks (modified after [124]). (b) Simplified regional geological map of the western margin of Yangtze Block showing the spatial-temporal distribution of Neoproterozoic plutonic complex (modified from [132]).

Yangtze Block, which is considered by some researchers as a Kangdian rift basin [6], with volcanic rocks of probably bimodal nature erupted at ca. 800–780 Ma [35–37]. It unconformably overlies the Yanbian Group and is covered by the Kaijianqiao Formation with a set of sandstones interlayered with tuff of SHRIMP age of 801–779 Ma [38, 39]. Although the outcrops of Neoproterozoic magmatic complexes are discontinuous, numerous U-Pb zircon ages suggest a continuous supra-subduction magmatism from ca. 860 to 750 Ma [11 and references therein].

The NE-striking Longmenshan Belt extends to a distance of about 500 km from the Xianshuihe fault in the southwest to Hanzhong in the northeast. The Longmenshan Belt separates the Songpan-Ganze turbidite basin and the Sichuan Meso-Cenozoic basin, which evolved from an oceanic basin to a continental setting during Late Triassic time [40]. It consists of Neoproterozoic intermediate-felsic intrusions and smaller mafic plutons (Figure 1(b)). Although the outcrops of Neoproterozoic magmatic complexes within the Longmenshan and other orogenic belts in the western Yangtze Block are discontinuous, the available numerous U-Pb zircon ages show a continuous magmatism from ca. 890 to 740 Ma [11, 41]. The regional stratigraphy successively, although with few interruptions, ranges from the Paleoproterozoic basement rocks of the Yangtze Block to the Cenozoic strata of the Sichuan basin. The Precambrian magmatic intrusions are dominated by compositionally diverse granites and diorites as, respectively, batholiths or stocks, and gabbroic stocks and dkes [42] (Figure 2). The Neoproterozoic magmatic rocks, in particular gabbroids and diorites, experienced strong deformation and low-grade metamorphism [43].

The study area is located in the central part of the Longmenshan Belt (Figure 1), and it is dominated by Neoproterozoic K-feldspar granitoids, diorites, and gabbroids (gabbro-diorite, gabbro) (Figures 2 and 3). In general, large dioritic plutons, like the ca. 860 Ma Guandaoshan intrusion, are rare in the western Yangtze Block. The Tianquan gabbroids and diorites under investigation occur as stocks or dykes (Figures 3(a)–3(e)). The relationships between gabbroids and granitoids are variable. The 3–5 meters thick NNE-striking gabbro and dolerite dykes often cut K-feldspar granites. In places, the gabbros are also intruded by leucocratic granitoids (Figure 3(f)). The diorites occur as larger outcrops located in the southwestern part of the study area (Figures 2 and 3(e)). Most contacts between different rock lithologies are covered by vegetation (Figure 3(b)). We sampled small stocks and dykes of gabbroids and diorite cropping out along the Da and Laba rivers (Figure

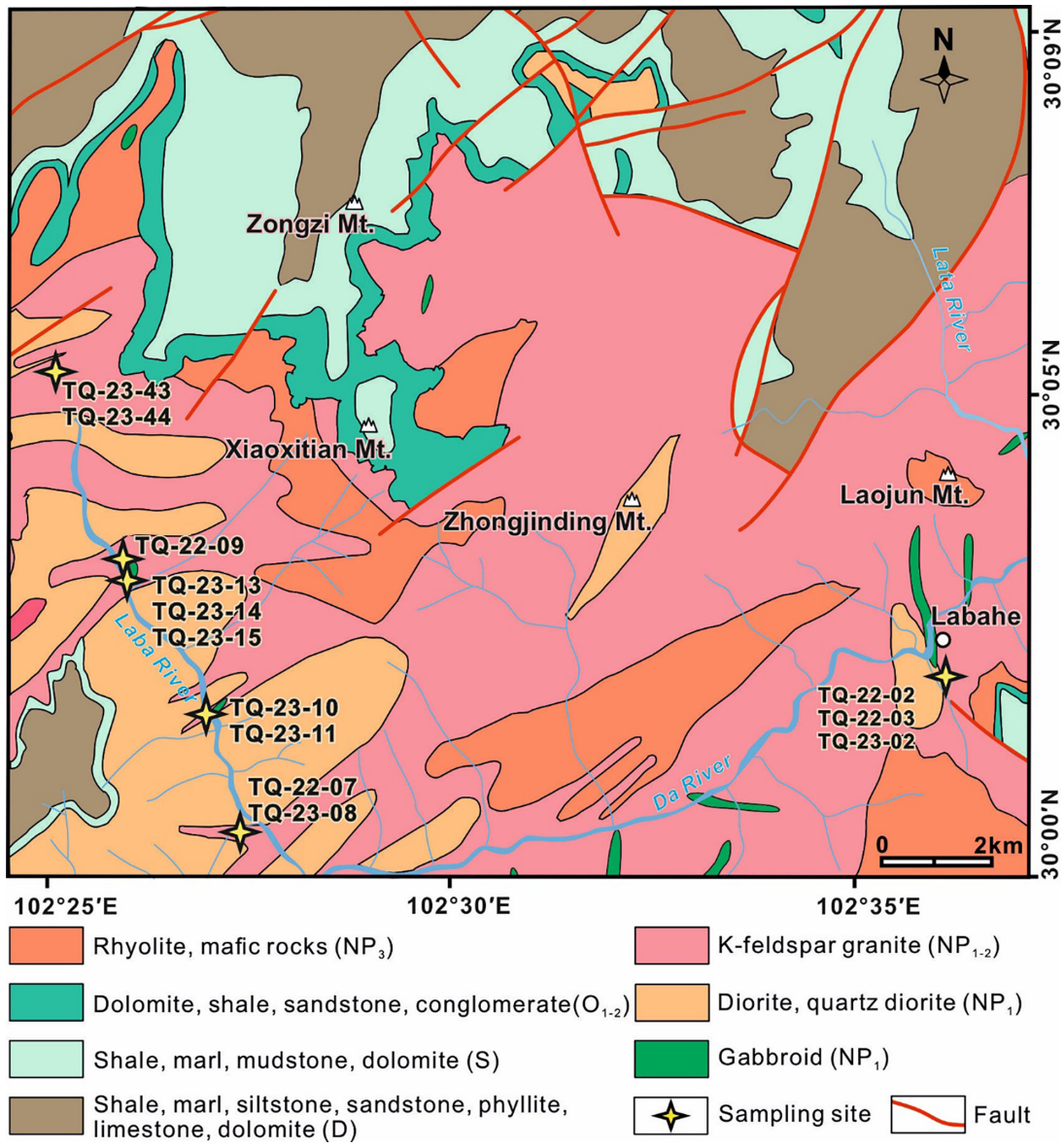

Figure 2: Schematic geological map of Tianquan County.

2). For the description of rock samples, see online supplementary table S1.

3. PETROGRAPHY

Petrographically, there have been identified three main types of rocks: gray monzo-gabbro, black to gray and greenish-gray gabbro (mostly amphibole-bearing), and gray diorite. Gabbro TQ-22-09 resembles monzo-gabbro as it has monzonitic structure with idiomorphic plagioclase (~50%), subidiomorphic alkaline feldspar (~15%), and amphibole (~35%) (Figure 4(a)). The other gabbros possess massive structure and typical gabbroic, intersertal, and subophitic or gabbro-ophitic textures that are well seen in both fist-size rock samples and thin sections Figures figures 3(a), 3(b) and 4(b)–4(d), . Greenish varieties are characterized by secondary alteration, first of all, chloritization and epidotization. The gabbros consist of plagioclase (45%–50%), clinopyroxene (25%–40%), hornblende (10%–15%), and accessory biotite, quartz, opaque minerals (probably magnetite), and zircon (Figures 4(b)–4(d)). A limited number of gabbroic samples contain olivine partly replaced by clinopyroxene and chlorite (Figure 4(c)). The 0.2–2 mm long plagioclase crystals are prismatic, euhedral to subhedral (Figures 4(a)–4(d)). The grains of clinopyroxene and hornblende are mostly idiomorphic. The colorless to pleochroically pink clinopyroxene grains are 0.1–1.5 mm in diameter. A part of clinopyroxene grains possesses a parallel cleavage typical of Ti-augite. The grains of amphibole (hornblende) also show pleochroism from light green to brown.

The diorites have massive structure, fine- to coarse-grained allotriomorphic and hypidiomorphic textures (Figures 3(c), 3(d), and 4(e)–4(f),). Fine- and

FIGURE 3: Representative field photos of Tianquan magmatic rocks: (a, b) gabbros; (c-e) diorites; (f) gabbro and leucocratic granite.

medium-grained diorites consist of plagioclase (55%–60%), hornblende (25%–35%), almost fully replaced by chlorite, K-feldspar (10%–15%), quartz (5%–10%), accessory biotite, apatite, and abundant opaque minerals (magnetite) and iron hydroxides (Figure 4(f)). More coarse-grained varieties of diorite consist of plagioclase (55%–60%), hornblende (15%–25%), K-feldspar (10%–15%), quartz (5%), accessory zircon and opaque minerals (Ti-magnetite) up to 0.25 mm in diameter. The grains of plagioclase and hornblende are subhedral-euhedral in shape (Figure 4(f)). The plagioclase grains are larger than those of hornblende and range in size from 0.4 to 1.2 mm. Hornblende is often replaced by secondary epidote and chlorite. Quartz grains are typically subhedral to anhedral.

4. RESULTS

4.1. Zircon U-Pb Dating

Among all the samples collected in the midstream of the Laba River and near Labahe Town online supplementary figure S1, three gabbros and three diorites were chosen for U-Pb zircon age dating (Figure 2), of which four new ages (gabbros TQ-22-09, TQ-23-10, TQ-23-13, and diorite

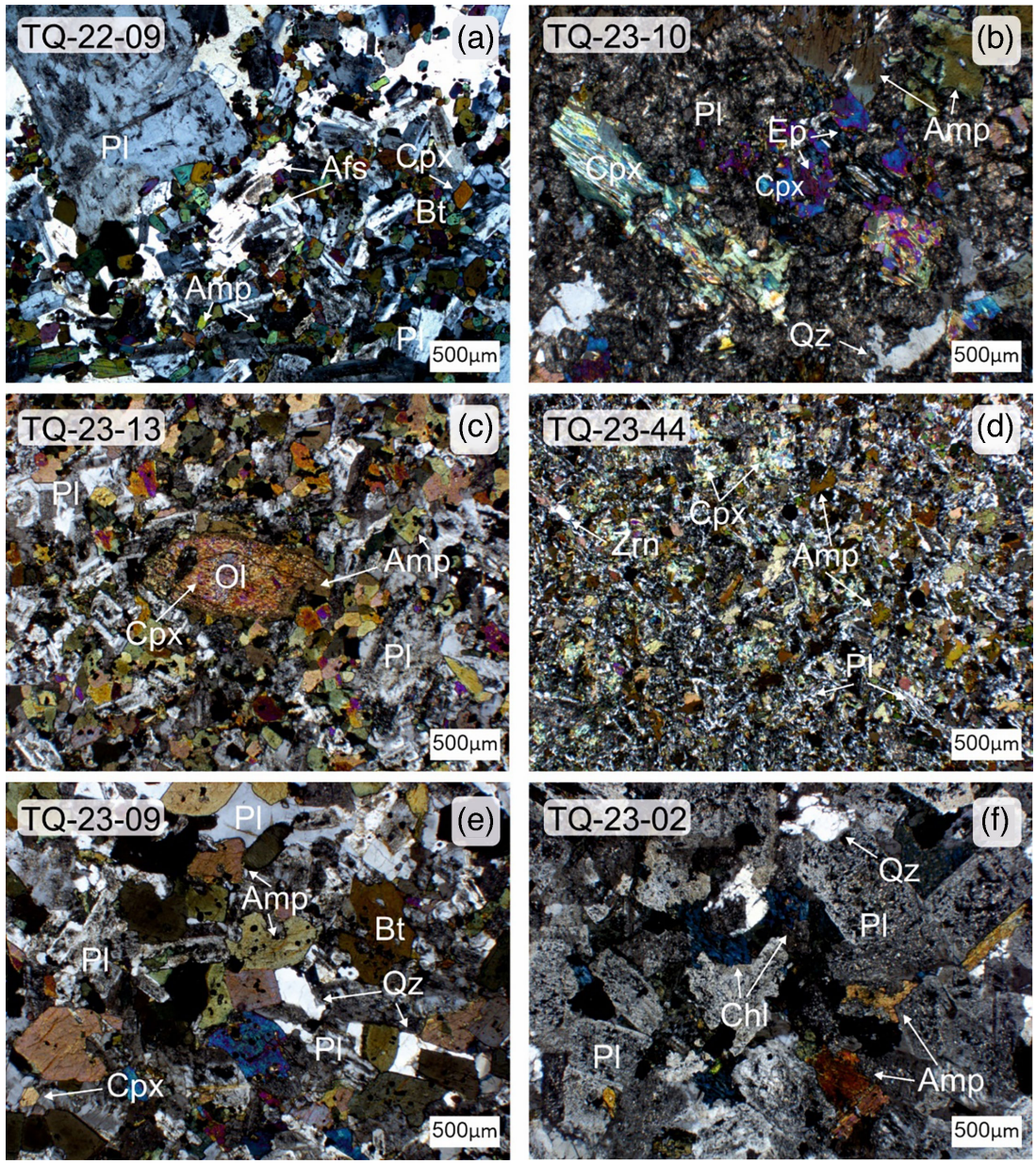

FIGURE 4: Representative photomicrographs of Tianquan gabbros (a–d) and diorite (e–f). Abbreviations: Ol, olivine; Cpx, clinopyroxene; Amp, amphibole; Pl, plagioclase; Afs, alkaline (K, Na) feldspar; Qz, quartz; Bt, biotite; Ep, epidote; Zrn, zircon.

TQ-23-02) are presented in this paper (online supplementary table S1) and two ages (TQ-23-07 and TQ-23-09) were reported in [44]. The zircons separated from the samples have sizes ranging from 180 to 310 μm in gabbros and from 110 to 230 μm in diorite. The grains are mostly colorless and transparent to translucent, subhedral to euhedral, stubby to prismatic (with aspect ratios of 1:1 to 3:1). For U-Pb age dating, the zircons were analyzed by LA-ICP MS (for details on the methodology, see Supplementary doc file). The results of the U-Pb dating are presented in Electronic Materials (online supplementary table S2). Cathodoluminescence images show that the most of the zircons have well-seen oscillatory zoning, less of them show sectorial zoning, and all lack visible inherited cores (online supplementary figure S2). The overwhelming majority of the zircon crystals used to determine the age of the rocks have Th/U ratios higher than 0.4, but lower than 1.7 (online supplementary table S2, online supplementary figure S3). Such Th/U ratios are typical of magmatic rocks [e.g. 45, 46]. All zircons yielded Neoproterozoic ages. Low concordant data (discordance >5%) were excluded from consideration.

The obtained U-Pb isotope ratios from 38 of 48 zircons from gabbro TQ-23-10 form a population of $^{206}Pb/^{238}U$ ages ranging from 832 ± 9 Ma to 792 ± 11 Ma (Figure 5(a)) with a weighted mean of 816 ± 4 Ma. In gabbro TQ-23-13, we analyzed 36 grains, of which 22 were selected for plotting (Figure 5(b)). The ages span the interval of 807.4 ± 6 to 778.4 ± 7 Ma at a weighted average of 790 ± 3 Ma. Almost all the data are concordant or nearly concordant (online supplementary table S2). Twenty-three U-Pb zircon ages of

36 were accepted for gabbro TQ-22-09; the ages range from 804 ± 8 to 780 ± 13 (Figure 5(c)) with a weighted mean of 796 ± 3 Ma. Thirty-six zircons from diorite TQ-23-02 were analyzed, of which 35 were selected for discussion. The zircons yielded $^{206}Pb/^{238}U$ ages ranging from 828 ± 8 to 785 ± 11 Ma with a weighted mean age of 808 ± 4 Ma (Figure 5(d)). Accordingly, for samples TQ-23-10 (gabbro), TQ-23-02 (diorite), TQ-22-09 (monzo-gabbro), and TQ-23-13 (gabbro), we accepted the values of ca. 816, 808, 796, and 790 Ma, respectively, as the ages of crystallization. In Figures 5(e) and 5(f), we show the concordia diagrams of two more samples of Tianquan diorite [44], which weighed average zircon ages (813 ± 7 and 804 ± 5 Ma) are above and below the 808 Ma age of diorite TQ-23-02 (Figure 5(d)).

In this paper, we present the first full major and trace-element data from Laba mafic plutonic rocks and new data from diorites exposed in the Tianquan County (Figure 2; for analytical data and grouping see online supplementary table S3). Details on the sampling and rock descriptions are available in online supplementary figure S1. The whole-rock geochemical data are illustrated in Figures 6–8. All samples are characterized by losses on ignition below 2 wt.% assuming their relatively fresh chemical compositions. The concentrations of major elements were re-counted to 100% anhydrous for inter-element comparisons and plotting. The plutonic rocks from all localities plot in the fields of gabbro, gabbro-diorite, and diorite in the TAS classification diagram (Figure 6(a)) and in the field of gabbro and diorite in the Zr/TiO_2 versus SiO_2 classification diagram (Figure 6(b)). The samples are dominated by subalkaline varieties although several samples are plotted at the boundaries between the tholeiitic and calc-alkaline fields (Figures 6(c) and 6(d)) and one sample plots in the tholeiitic field (Figure 6(c)). Gabbros TQ-23-13 and TQ-22-09 represent alkaline rock, monzo-diorite (alkaline gabbro-diorite), and monzo-gabbro, respectively (see section 3; Figure 6(a)). In the SiO_2 versus K_2O diagram, the diorites form two groups showing different ranges of the concentrations of K_2O (Figure 6(d)).

4.2. Whole-Rock Major and Trace Elements

The subalkaline gabbros are characterized by SiO_2 contents spanning 47.2–52.4 wt.%, high CaO = 6.7–9.6 wt.%, medium MgO = 4.2–8.3 wt.%, Na_2O = 2.4–4.6 wt.%, and K_2O = 1.1–2.3 wt.%. The Mg# values [(MgO/(MgO + FeO_T)×100] range from 36.7 to 60.1. In the Harker variation diagrams (Figure 7), the rocks form one or two trends, except for the alkaline gabbro. The subalkaline gabbros display negative correlation between SiO_2 and MgO, Fe_2O_{3T}, CaO, Na_2O, and, partly, Ni, suggesting fractionation of olivine and pyroxenes (Figures 7(a)–7(e)). In the SiO_2–Al_2O_3 diagram, the diorites again form two groups: the low-alumina diorites form a trend with higher Mg-Fe gabbros (Figure 7(f)) and the high-Al diorites are also characterized by higher contents of K_2O (Figure 6(d)). In the SiO_2 – ΣLREE (total light rare-earth elements) diagram, the gabbros plot as three groups variably enriched in the REE suggesting different mantle sources or fractionation of garnet (Figure 7(g)). A part of gabbros and diorites forms a single positive trend, that is the ΣLREE increase with increasing SiO_2 indicating a successive melt evolution, that is enrichment of residual melts during fractionation (Figure 7(g)). Two samples of gabbro have higher ΣREE (119.7 and 126.5) compared to the gabbros that form single trends with diorites with ΣREE ranging from 43.8 to 73.4 ppm and, accordingly, hereinafter they will be referred to as "Group 1 – normal gabbro" (Mg# = 47.9–60.1) and "Group 2 – enriched gabbro" (Mg# = 50.2–57.3). Gabbro TQ-23-13 is the youngest (790 ± 3 Ma; Figure 5(b)) we consider separately because unlike the Group 1 gabbros it is more alkaline (Figure 6(c)) and is characterized by increased TiO_2 (Figure 7(h)) and ΣREE (Figure 7(g)). Accordingly, hereinafter, we will call it "high-Ti gabbro."

Group 1 gabbros and the high-Ti gabbro TQ-23-13 are characterized by LREE-enriched, moderately differentiated HREE (La/Yb_N = 2.9–3.7; La/Sm_N = 1.5–1.8; Gd/Yb_N = 1.4–1.7) and show weak negative to positive Eu anomalies (Eu/Eu^* = 0.9–1.1) (Figure 8(a)). Their primitive-mantle-normalized spidergrams possess clear depletions in high-field strength elements (HFSE), in particular, Nb and Ta, relative to Th and La (Nb/Th_{pm} = 0.2–0.7; Nb/La_{pm} = 0.2–0.4) (Figure 8(b)). The REE pattern and sidergram of the high-Ti gabbro are higher than those of Group 1 gabbros. Group 2 gabbros are more enriched in the LREE (La/Yb_N = 9.4–10.8; La/Sm_N = 2.7–2.8), have more differentiated HREE (Gd/Yb_N = 2.2–2.5) and negligible negative Eu anomalies (Eu/Eu^* = 0.9–1.0) (Figure 8(a)). Their spidergrams show enrichment in large ion lithophile elements (LILEs, e.g. Rb, Ba) and troughs at Nb-Ta (Nb/Th_{pm} = 0.2–0.4, Nb/La_{pm} = 0.3–0.4) and Ti (Ti/Ti^* = 0.4–0.8) (Figure 8(b)).

The gabbro-diorites and diorites have SiO_2 contents spanning 55.7–61.0 wt.% and Na_2O + K_2O from 5.3 to 6.7 wt.% (Figure 6(a) and 6(b)). The contents of CaO (2.6, 6.8 wt.%), $^{T}Fe_2O_3$ (6.4, 11.4 wt.%), MgO (2.3, 4.4 wt.%) are also, like in case of a part of gabbroids, negatively correlated with SiO_2 contents (Figures 7(a)–7(c)). The Mg# numbers of diorites are relatively low ranging from 33.1 to 45.1. There are two groups of diorites according to the contents of Al_2O_3 and K_2O: Group 1 diorites (Al_2O_3 = 13.6–14.4, K_2O = 1.1–1.5 wt.%) [44] and new diorites hereinafter referred to as Group 3 (Al_2O_3 = 15.9–17.7, K_2O = 1.5–2.2 wt.%) (Figures 6(d) and 7(e)). The shapes of the REE patterns of the diorites of both groups are similar: moderately enriched in the LREE (La/Yb_N = 2.9–6.2), and, similarly to Group 1 gabbros, they show a depletion of HREE relative to middle REE (Gd/Yb_N = 1.0–1.8) and weak negative to positive Eu anomalies (Eu/Eu^* = 0.8–1.2; Figure 8(c)). The spidergrams of both groups of diorites are also similar displaying negative Ta-Nb anomalies (Nb/Th_{pm} = 0.2–0.6, Nb/La_{pm} = 0.3–0.4) and troughs at Ti (Figure 8d; online supplementary table S3). However, compared to Group 3 diorites, Group 1 diorites show lower ΣREE (102.9, 132.8; Figure 8(c)), La/Sm_N (1.7, 2.4), La/Yb_N (3.1, 5.9) and Gd/Yb_N (1.4,

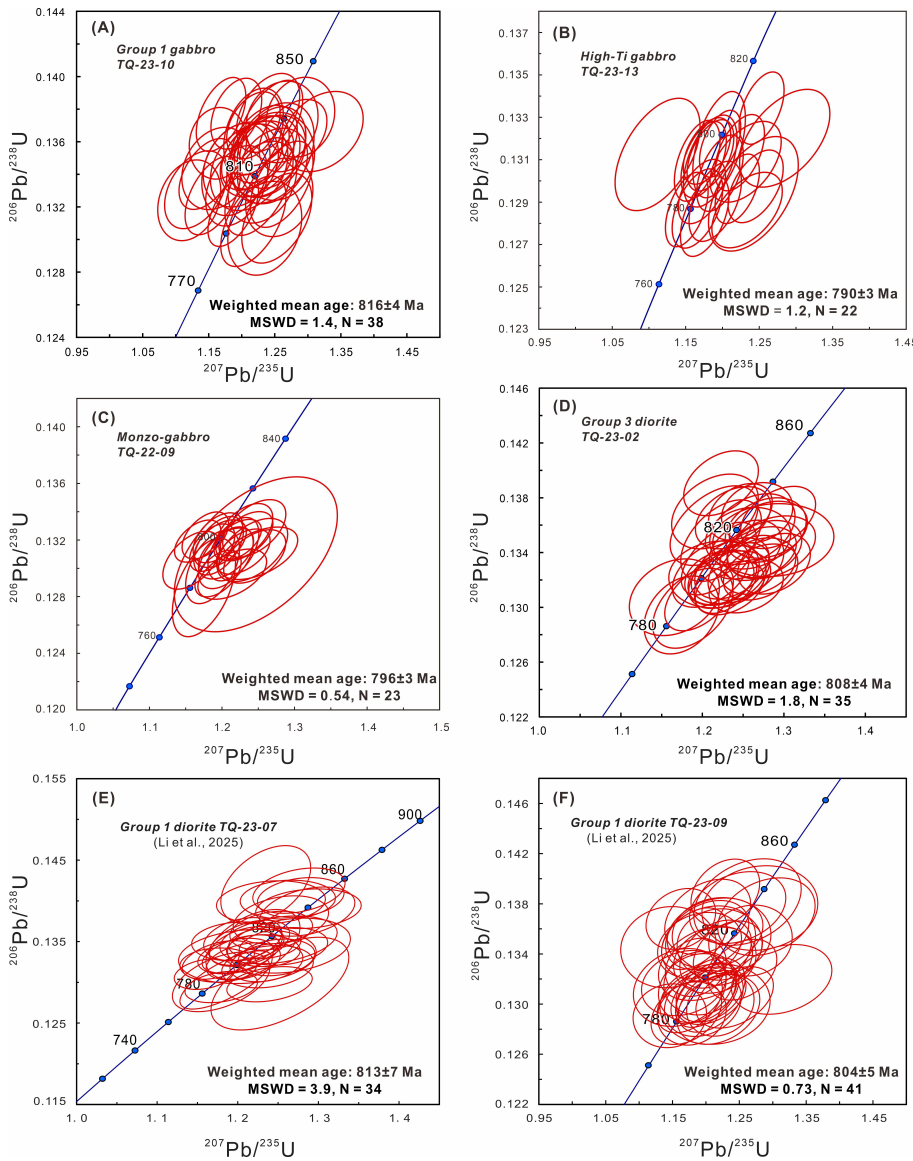

FIGURE 5: Concordia diagrams with results of U–Pb zircon dating of Tianquan gabbros and diorites: (A)–(D), new data; (E) and (F), from Tianquan diorites of the same area reported in [44].

1.7), but higher Nb/Th_{pm} (0.38, 0.24; Figure 8(d)) (online supplementary table S1).

Thus, Group 1 gabbros and Group 1 diorites form single trends in most Harker's diagrams (Figure 7), most of which fit the global evolutionary trends based on major oxides of arc plutonic rocks [46]. Group 1 gabbro and diorites show typical island-arc spidergrams with enrichments in LILEs (Rb, Ba; online supplementary table S3) and depletions in HFSE (Nb, Ta, and Ti) (Figures 8(b) and 8(d)). Group 2 gabbros are characterized by higher TiO_2 and LREE, and more differentiated HREE (Figure 8(a)), but their spidergrams also display troughs at Nb-Ta and Ti (Figure 8(b)). The high-Ti gabbro is different from Group 2 gabbros by lower LREE (Figure 8(a)). Group 3 diorites are different from Group 1 diorites in higher Al_2O_3, K_2O, La/Sm_N, La/Yb_N, and Gd/Yb_N, but lower ΣREE (129, 179 ppm) and Nb/Th_{pm}. The monzo-gabbro TQ-22-09 that is characterized by high total alkali (Na_2O+K_2O = 5.9 wt.%), medium Mg# (38), higher ΣREE (168 ppm). Accordingly, its REE pattern takes the highest position (Figure 8(a); La/Yb_N = 9.7; La/Sm_N = 2.4) and shows highly differentiated HREE (Gd/Yb_N = 2.7). The TQ-22-09 spidergram is characterized by the absence of a notable trough at Nb-Ta (Figure 8(b)).

4.3. Zircon Lu-Hf and Whole-Rock Sm-Nd Isotope Data

In this paper, we present first Hf-in-zircon and whole-rock Sm-Nd isotope data from Tianquan mafic magmatic rocks (Group 1 gabbros and monzo-gabbro; Figures 6–8; online supplementary tables S4 and S5) and new data from diorites (Group 3) exposed in the Tianquan County of the western Yangtze Block in coordination with the published isotope data from Group 1 diorites [44]. For the details on the

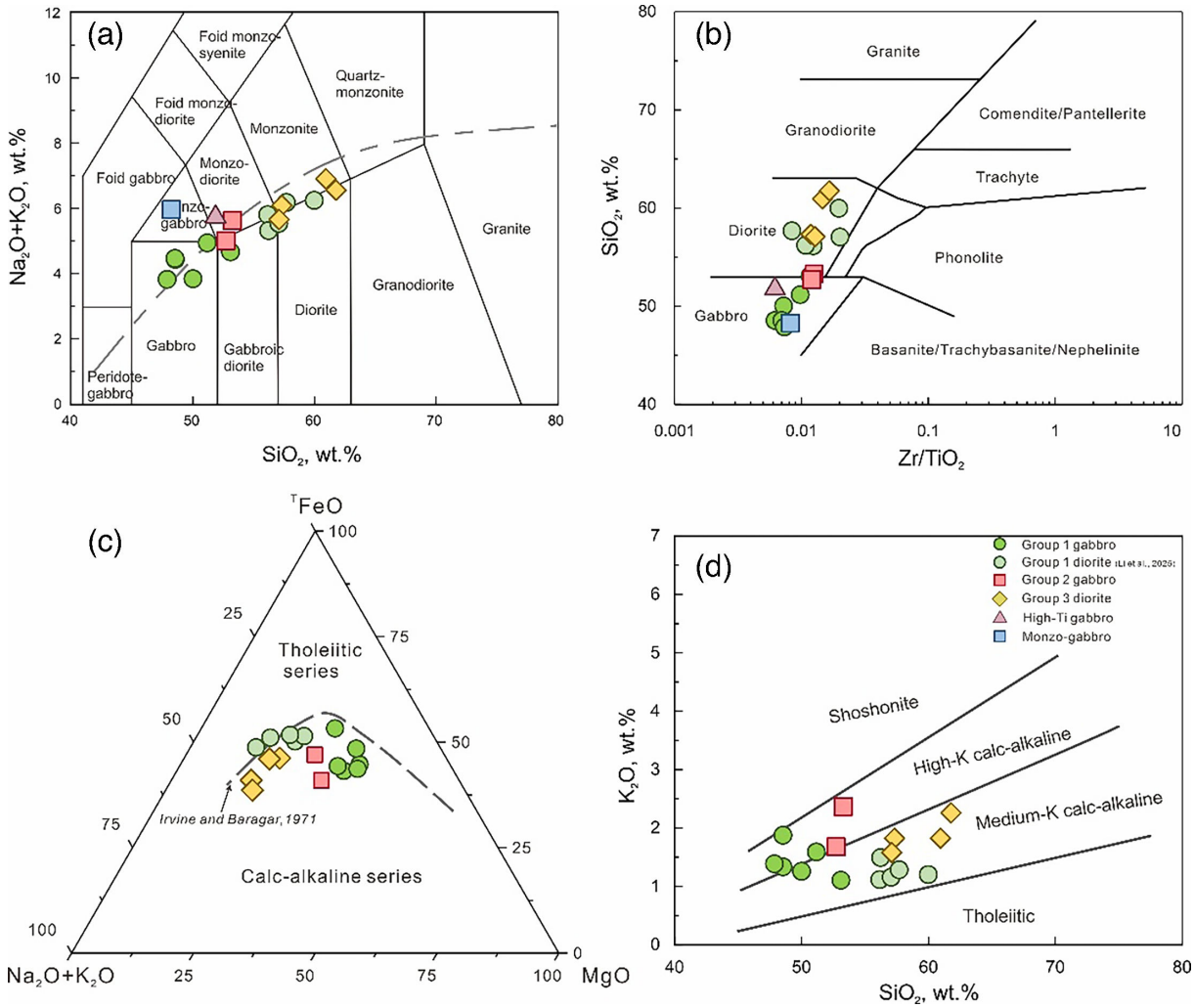

FIGURE 6: Geochemical classification diagrams of Tianquan magmatic rocks: (a) silica versus total alkali (TAS) diagram after [133]; (b) Zr/TiO_2 versus SiO_2 diagram [134]; (c) Na_2O+K_2O-FeO_t-MgO ternary diagram [135]; (d) SiO_2 versus K_2O diagram [136].

methodology of isotope analyzes see Supplementary doc file. To calculate the initial isotope ratios, we used the weighted mean U–Pb zircon ages of the targeted samples (Figure 5; online supplementary table S2).

4.3.1. Lu-Hf Isotope Systematics

Analysis of the Lu-Hf isotope system in magmatic zircons is traditionally applied to understand the origin and evolution of parental magmatic melts through tracking fractionation of elements having affinities to crust or mantle to conclude if the mantle source was juvenile or contained recycled crustal material [47, 48]. For *in situ* Lu-Hf isotope analysis, we chose zircon grains from three samples of gabbro (Group 1 gabbro TQ-23-10, high-Ti gabbro TQ-23-13, and monzo-gabbro TQ-22-09) and one sample of diorite (TQ-23-02), which yielded concordant U-Pb ages (Figure 5; online supplementary table S4). The laser shooting for the Hf-in-zircon analysis was made at the grain segments that are located near the craters made during the U-Pb isotope dating (online supplementary figure S2).

Ten zircons from Group 1 gabbro TQ-23-10 yielded the $^{176}Lu/^{177}Hf$ ratios of 0.000513 to 0.002328 with an average of 0.001212, the $^{176}Hf/^{177}Hf$ ratios of 0.282540 to 0.282605 with an average of 0.282572, and consistently positive $\varepsilon Hf_{(t)}$ values of +9.4 to +11.3 with an average of +10.3 (Figure 9(a); online supplementary table S4). The recalculated two-stage Hf model age relative to the depleted mantle (DM) (T_{DM2}) ranges from 1111 to 1024 Ma.

Six zircons from high-Ti gabbro TQ-23-13 yielded the $^{176}Lu/^{177}Hf$ ratios of 0.003229 to 0.005828 with an average of 0.004844 and the $^{176}Hf/^{177}Hf$ ratios of 0.282613 to 0.282715 with an average of 0.282663. The related $\varepsilon Hf_{(t)}$ values are all positive ranging from +9.2 to +12.6 with an average of +11.0 indicating a highly depleted mantle source (Figure 9(a)). The two-stage Hf model ages (T_{DM2}) span 1099–903 Ma.

Six zircons from monzo-gabbro TQ-22-09 yielded the $^{176}Lu/^{177}Hf$ ratios of 0.000188 to 0.005862 with an average of 0.004399, the $^{176}Hf/^{177}Hf$ ratios of 0.282744 to 0.282914 with an average of 0.282831, and accordingly positive $\varepsilon Hf_{(t)}$ values of +14.0 to +21.2 with an average of +17.3 (Figure

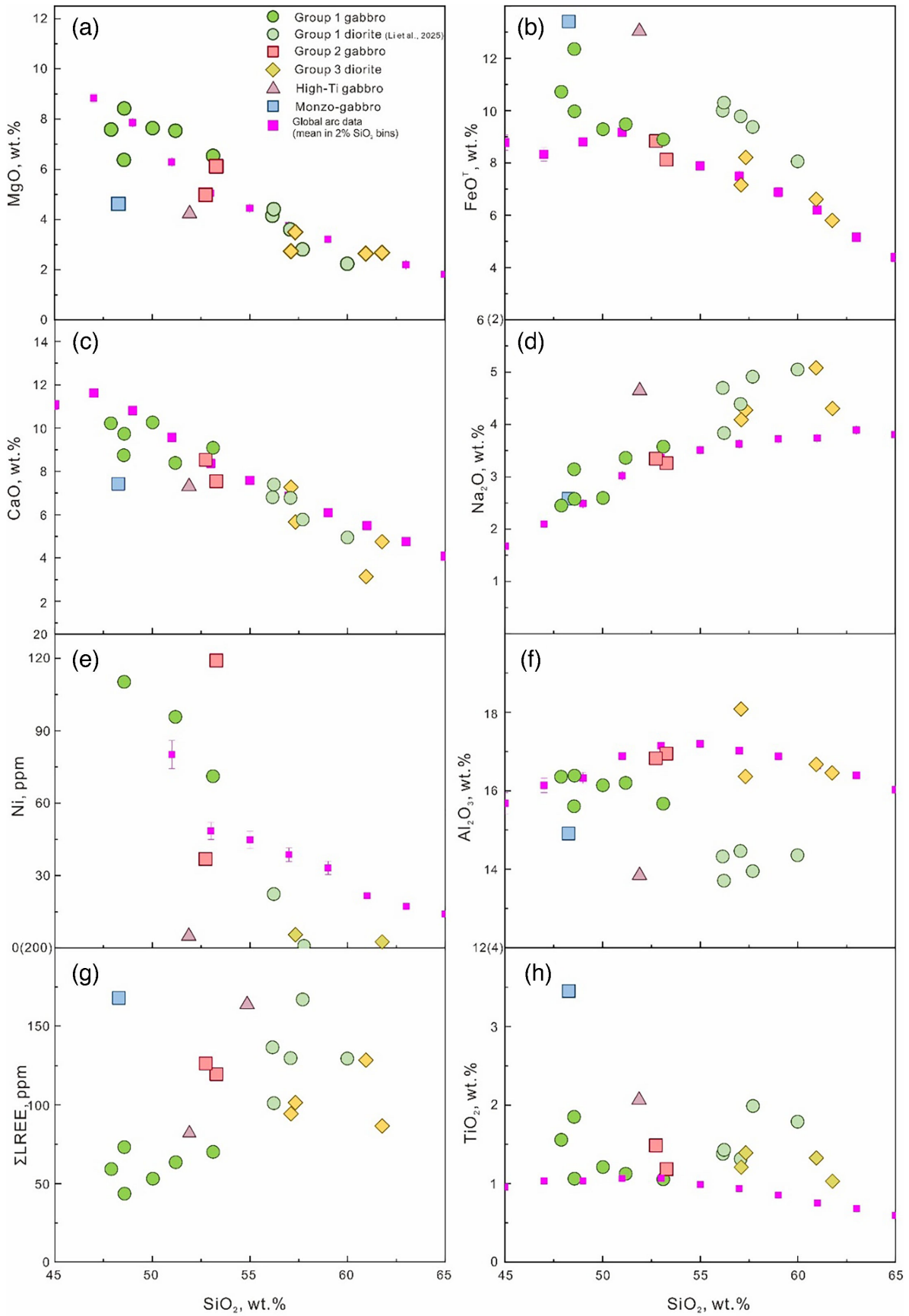

FIGURE 7: Harker diagrams of major oxides and trace elements of Tianquan magmatic rocks in comparison with the data from global arc plutonic rocks shown in pink squares [137].

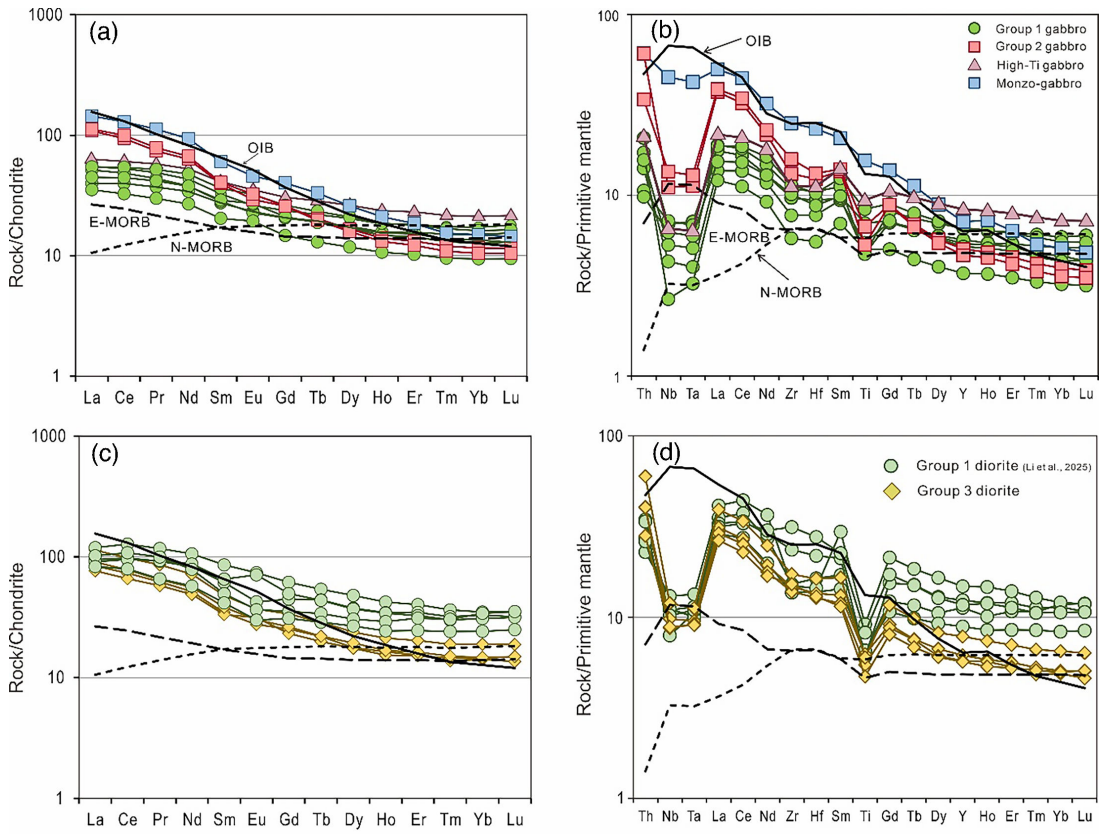

FIGURE 8: (a), (c) chondrite-normalized rare-earth element (REE) patterns; (b), (d) primitive mantle-normalized trace-element spider diagrams for Tianquan magmatic rocks. Normalization values are after [89].

9(a)). Two values of $\varepsilon Hf_{(t)}$ appeared extremely high, and the related values of T_{DM1} appeared unrealistic because younger than the ages of the zircons; therefore, these grains were excluded from further consideration. The values of T_{DM2} for the other four grains are closer to the ages of crystallization of the monzo-gabbro (ca. 796 Ma) implying an extremely depleted or metasomatized magma source [49].

Ten zircon grains from Group 3 diorite TQ-23-02 yielded $^{176}Lu/^{177}Hf$ ratios ranging from 0.001455 to 0.007928 with an average of 0.005114 and $^{176}Hf/^{177}Hf$ ratios of 0.282567 to 0.282745 with an average of 0.282656. The related values of $\varepsilon Hf_{(t)}$ span +9.5 to +12.9 with an average of +11.1, and the T_{DM2} ages vary from 1072 to 874 Ma. The values of $\varepsilon Hf_{(t)}$ for Group 3 diorite overlap with those of Group 1 diorites [44] and Group 1 gabbro (Figure 9(a)), suggesting that the parental magmas of magmatic rocks of both groups were derived from a single depleted mantle source. The values of T_{DM2} for all samples except the monzo-gabbro are slightly older than the ages of crystallization that are typical of juvenile mantle sources.

4.3.2. Sm-Nd Isotope Systematics

Whole-rock Sm–Nd isotopic compositions of magmatic rocks are typically used to estimate the modal age and juvenile or recycled character of their mantle sources. Four Group 1 gabbroic samples, Group 3 diorite (TQ-23-02), high-Ti gabbro, and monzo-gabbro were analyzed for Sm and Nd isotope ratios (online supplementary table S5). The previously published data from Group 1 diorites [44] were also included into the dataset and plotted on isotope diagrams for comparison (Figures 9(a)–9(c)). The Group 1 gabbroic samples have Sm = 4.46-5.26 and Nd = 18.3-21.4 ppm, similar to those of Groups 1 and 3 diorite (Sm = 4.58, Nd = 21.0 ppm), but higher $^{143}Nd/^{144}Nd$ (0.512535, 0.512603) than the Group 3 diorite ($^{143}Nd/^{144}Nd$ = 0.512394). The concentrations of Sm and Nd in the monzo-gabbro are higher than in all other samples, but its $^{147}Sm/^{144}Nd$ ratio is the lowest. The age versus $\varepsilon Nd_{(t)}$ covariation diagram (Figure 9(b)) shows that all samples are characterized by positive values of $\varepsilon Nd_{(t)}$. The highest εNd_t value indicating a more depleted mantle source was recorded for the monzo-gabbro (+6.08). Group 3 diorite yielded the lowest $\varepsilon Nd_{(t)}$ of +1.93. The Group 1 gabbros and diorites and the high-Ti gabbro have similar values of $\varepsilon Nd_{(t)}$ ranging from $_{+}$3.1 to +4.4 suggesting similar mantle sources. The two-stage Nd model ages are 1243–1126 Ma for Group 1 gabbros and diorites, 1336 Ma for Group 3 diorite, and 997 Ma for monzo-gabbro. All isotopic parameters from Group 1 diorites [44] match those of Group 1 gabbros. The age versus $\varepsilon Nd_{(t)}$ diagram (Figure 9(b)) demonstrates that the parental melts of the rocks under study were derived from a mixed mantle source (Group 3 diorite), depleted/juvenile mantle sources (Group 1 gabbros and diorites and high-Ti gabbro) and

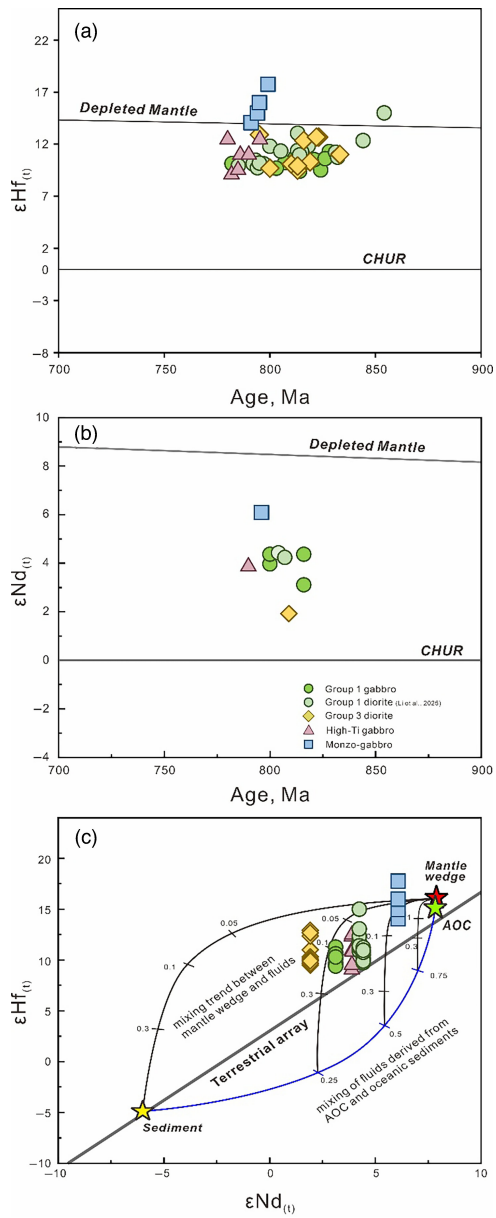

FIGURE 9: (a) Age versus εNd_t; (b) age versus εHf_t, and (c) εNd_t versus εHf_t versus isotope diagrams for the Tianquan magmatic rocks illustrating mixing between mantle wedge, subducted altered oceanic crust (AOC), and sediment-derived melts after [138]. Blue line in panel C indicates mixing of AOC-derived and sediment-derived fluids; solid black lines indicate mixing of fluids or melts and mantle wedge. The terrestrial array in panel C is after [139].

from an extremely depleted or metasomatized mantle source (monzo-gabbro). The juvenile source or sources were possibly slightly contaminated by crustal material to produce the $\varepsilon Nd_{(t)}$ values plotted more away from the DM line, that is not as positive as $\varepsilon Hf_{(t)}$ (Figure 9(a)).

5. DISCUSSION

5.1. Age Constraints on the Emplacement of Tianquan Magmatic Rocks

The Neoproterozoic magmatic formations exposed in the western Yangtze Block were formed during a long period from ca. 890 to 740 Ma [11 and references cited therein] (Figures 1 and 2). Two major episodes of the Neoproterozoic magmatism have been recognized: 890–860 and 830–740 Ma [10]. The main rock series are (1) 890–840 Ma calc-alkaline gabbro-gabbro-diorite and diorite [e.g. 15, 50], (2) 870–750 calc-alkaline to alkaline diorite-monzonite-granite [e.g. 2, 51], (3) 780–750 adakites and volcanic rocks [e.g. 8, 52]. In the Tianquan County, the direct contacts between the rocks of the first 2 series are typically concealed (Figures 3(a)–3(e)); however, in places, we can see how the granitoids of the alkaline series often intrude the older gabbroids (Figure 3(f)).

Of special interest are the 870–780 Ma gabbroic intrusions exposed discontinuously along the entire western Yangtze Block from north to south [15] (Figure 1). In the Hannan region of the NW Yangtze Block, the mafic magmatic formations include 820–784 Ma Wangjiangshan olivine gabbro, ca. 814 Ma Beiba olivine gabbro, ca. 780 Ma Bijigou hornblende gabbro, and ca. 746 Ma Luojiaba hornblende gabbro [7, 50, 53–55]. In the western Yangtze Block, there are ca. 877 Ma Liujiaping gabbro, 870–850 Ma Baoxing gabbro, 820–800 Ma gabbro, and ca. 837 Ma diabase of the Shimian ophiolite belt, ca. 820 Ma and 790 Ma mafic dykes of the Mianning region and 780–760 Ma hornblende gabbro of the Longmenshan Belt [15, 25, 28, 56–59]. The numerous gabbroic exposures of the SW Yangtze Block include ca. 857 Ma Ganyuhe hornblende gabbro [60], ca. 856 Ma Guandaoshan and Tongde gabbro [15, 61], ca. 843 Ma Gaojiacun gabbro [15], ca. 837 Ma Lengshuiqing gabbro [15], ca. 823 Ma Dadukou gabbro [15], ca. 810 Ma Dajianshan gabbro-diorite [62], and ca. 787 Ma Shaba gabbro of the Panzhihua region [15] (online supplementary table S6).

Our new U-Pb zircon data from zircons from three gabbros and diorite of the Tianquan County, which is in the southern part of the Longmenshan Belt, yielded mean ages of 816, 796, 790, and 808 Ma, respectively. The youngest are the high-Ti gabbro (790 Ma) and the monzo-gabbro (796 Ma) (Figure 5). The data plus the ages of 807 and 804 Ma from [44] all suggest that the magmatism in the central part of the western Yangtze margin continued at least 25 Ma, from 816 to 790 Ma (Figure 5). In general, these data accord well with the previous overall age estimations for the Neoproterozoic magmatism of the western Yangtze Block (Figure 1), for example, with the 890–740 Ma period estimated in the western Yangtze Block, Panzhihua-Yuanjiang area [63], and with the 840–740 Ma zircon ages of magmatic rocks of the Kangdian rift located south of the study area [10, 37]. However, only the ages from Group 1 gabbros and diorites (816, 813, 808, and 804 Ma) are consistent with the previously published U-Pb isotope zircon ages of mafic magmatic rocks: 820–800 Ma gabbroids of the Shimian ophiolite belt, ca. 820 Ma mafic dykes of the Mianning region, and ca. 810 Ma Dajianshan gabbro-diorite [25, 28, 61, 63]. No such young ages as 796 Ma (monzo-gabbro) and 790 Ma (high-Ti gabbro) have been reported for the central part of western Yangtze before. A summary

histogram of U-Pb ages of zircons from gabbroids (Figure 10(a)) and diorites (Figure 10(b)) of the entire western Yangtze margin shows peaks at 860–850, 830–810, 800–780, and 760–740 Ma and troughs at 850–830 and 780–770 Ma for gabbroids and peaks at 860–850, 830–820, 810–800, and 760–740 Ma and troughs at 850–830 and 780–770 Ma for diorites (online supplementary table S6). The main peaks of magmatism, both mafic and intermediate, happened at 860–850, 830–810, and 760–740 Ma. Our new dates from Tianquan gabbros match the 830–810 and 800–780 Ma peaks and the new dates from Tianquan diorites (813, 809, and 804 Ma) discussed in this paper plus those from [44] match the 810–800 Ma peak (Figure 5).

5.2. Petrogenesis of Tianquan Gabbro and Diorites

Implications on the origin of Precambrian to early Paleozoic mafic igneous rocks compared to their actualistic analogs should be done with caution because of a probable change of the primary concentrations of mobile elements, such as Rb, Sr, Ba, Pb, K, and isotope ratios of Sr and Pb during post-magmatic alteration [e.g. 64–66]. Therefore, discussions of the petrogenesis and tectonic settings of the Neoproterozoic rocks under study, in particular, those of mafic composition, must be preferably based on immobile incompatible elements, in particular LREE and HFSE [e.g. 67–69]. It has been widely accepted that HFSE and, in particular, their element ratios, like Nb/Th and Zr/Y, are immobile during alteration or metamorphism and therefore represent valuable tools for understanding element mobility during geological processes [e.g. 70–72]. In Tianquan gabbros, Nb/Th = 1.3–5.7 and Zr/Y = 4.0–4.8 for Group 1 and Nb/Th = 1.5–3.4 and Zr/Y = 6.4–8.3 for Group 2 (online supplementary table S7 and online supplementary figure S5). These are comparable with the ranges of the average values of Nb/Th and Zr/Y from global intra-oceanic (Nb/Th = 1.8–2.5, Zr/Y = 2.9–3.0) and continental (Nb/Th = 2.8–6.2, Zr/Y = 2.3–7.7) magmatic arcs [73].

5.2.1. Fractional Crystallization and Mantle Sources

The Tianquan gabbroids and diorites typically occur as stocks and dykes; however, their contacts are seldom observed due to dense bamboo forest vegetation. Most of the samples under study possess geochemical features of calc-alkaline magmatic series except for monzo-gabbro and high-Ti gabbro (Figures 6(a) and 6(c)). In most geochemical diagrams based on major elements, the Group 1 gabbroids form single trends with Group 1 diorites suggesting fractionation of olivine and/or orthopyroxene and clinopyroxene (Figures 6(a), 6(b), and 7), but not amphibole because there is no correlation between SiO_2 and HREE (online supplementary figure S4). The weak fractionation of HREE and Eu ($Eu/Eu^* \sim 0.9 \pm 0.1$) may indicate a minor to nil fractionation of garnet and plagioclase, respectively (Figure 8(a); online supplementary figure S4). Evidence for the fractionation of Fe-Ti oxides comes from the negative correlation between SiO_2 and FeO^T (Figure 7(b)) and Nb-Ta and Ti minimums in the spidergrams ($Ti/Ti^* = 0.42–0.79$; Figure 8(b); online supplementary table S3). However, in the diagrams based on trace elements, Group 2 gabbros and monzo-gabbro plot away from the general trend of crystallization (Figure 7(g)) suggesting another scenario of petrogenesis, that is different mantle sources or different trends of fractionation.

The Hf-in-zircon and whole-rock Nd isotope systematics show that the melts, which crystallization formed Group 1 gabbros and diorites, monzo-gabbro, and Group 3 diorites, were derived by partial melting of depleted/juvenile mantle sources (Figures 9(a) and 9(b)) with participation of fluids derived from both altered oceanic crust (AOC) and subducted sediments (Figure 9(c)). The parental melts of Group 1 gabbros and diorites derived from the mantle wedge were mixed with 5%–15% of the fluids, of which possibly 25%–40% came from the AOC and 60%–75% from the subducted sediments. More evidence for the participation of subducted sediments in the petrogenesis of Group 1 gabbros and diorites comes from the Th/Yb versus Ba/La and La/Sm versus Ba/Th trace-element systematics (Figure 11) showing increased Ba and indicating that the petrogenesis of these rocks involved significant participation of the fluids derived from the dehydration of subducted oceanic slab.

The Lu-Hf and Sm-Nd isotope systematics of the monzo-gabbro show that its parental melt was derived from a highly depleted and almost dry mantle wedge source with a limited participation of fluids, less than 10%, of which 30% came from the subducted sediments and 70% from AOC (Figure 9(c)). On the contrary, the petrogenesis of Group 2 gabbros involved larger addition of subducted sediments than slab-derived fluids (Figure 11). The Group 3 diorites were derived from melts mixed with 3%–15% of the fluids, of which approximately 22% came from the AOC and 78% from the subducted sediments (Figure 9(c)).

In addition to the effect of fluids on the petrogenesis and participation of sediments, the trace-element geochemistry shows that the parental melts of Group 1 gabbroids and diorites, Group 2 gabbros, Group 3 diorites, high-Ti gabbro, and monzo-gabbro were derived from different mantle sources. Evidence for that comes from different enrichment in LREE and different degree of fractionation of HREE (Figures 8(a) and 8(c); online supplementary table S3). Group 1 gabbroids and diorites and high-Ti gabbro formed from similar sources ($La/Sm_N = 1.5–1.8$; $Gd/Yb_N = 1.4–1.5$; $La/Yb_N = 3.0–3.3$). Another type of sources gave Group 2 enriched gabbros and monzo-gabbro ($La/Sm_N = 2.4–2.7$; $Gd/Yb_N = 2.2–2.7$; $La/Yb_N = 9.4–10.8$). A mantle source that produced parental melts of Group 3 diorites was more enriched in the LREE but possessed less differentiated HREE ($La/Sm_N = 2.3–2.4$; $Gd/Yb_N = 1.6–1.8$; $La/Yb_N = 5.3–6.2$).

5.2.2. Geochemical Modeling

For more detailed implications on mantle sources, their composition, and degree of melting, we performed geochemical modeling based on trace elements of variable incompatibility in two systems, La/Sm_N versus Sm/Yb_N and Nb/Yb versus Yb (Figure 12). The melting curves

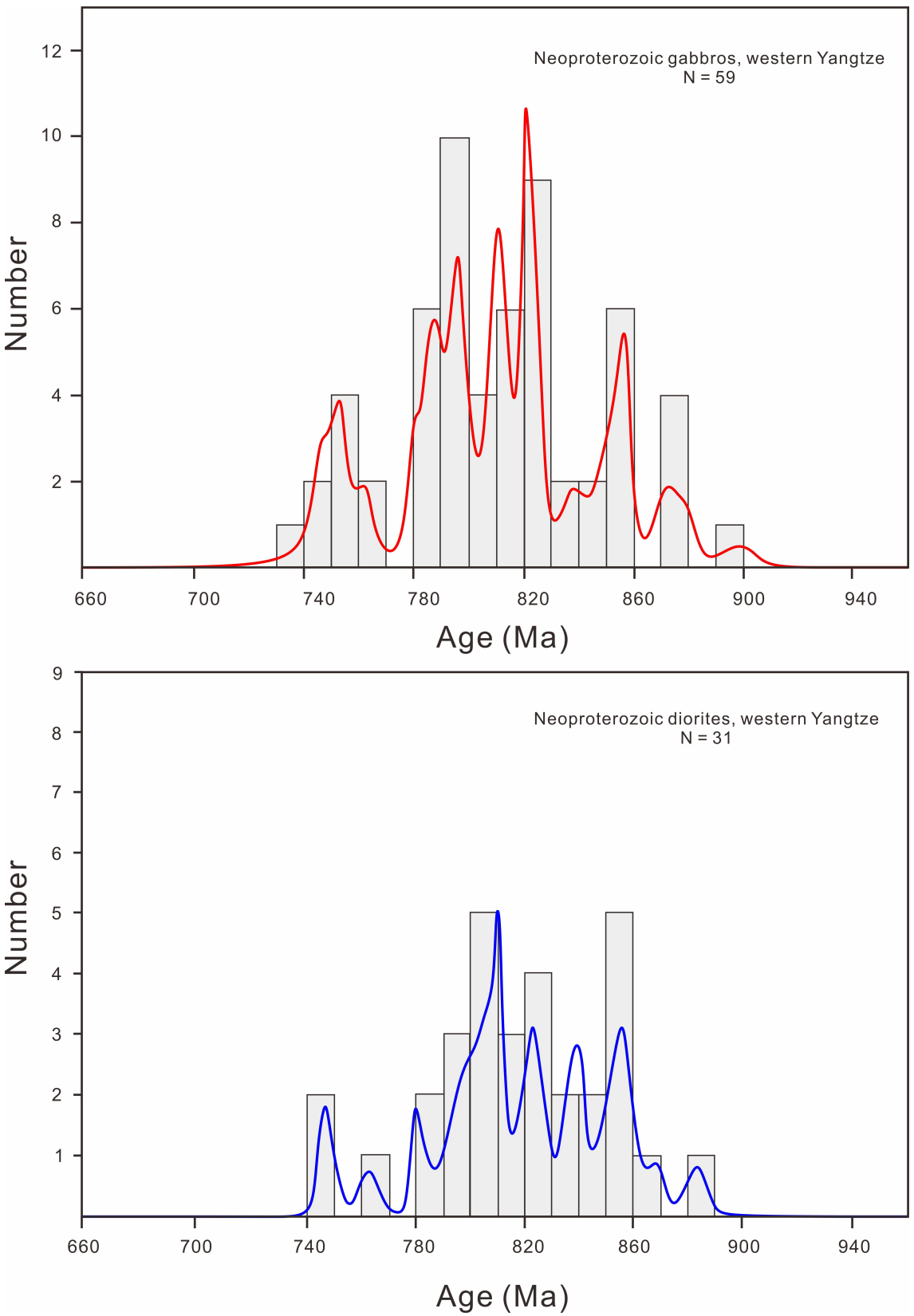

Figure 10: A summary histogram of U-Pb ages of zircons from gabbroids and diorites of the western Yangtze Block. Data sources: this paper [7, 8, 15, 25, 41, 50, 61, 62, 140],

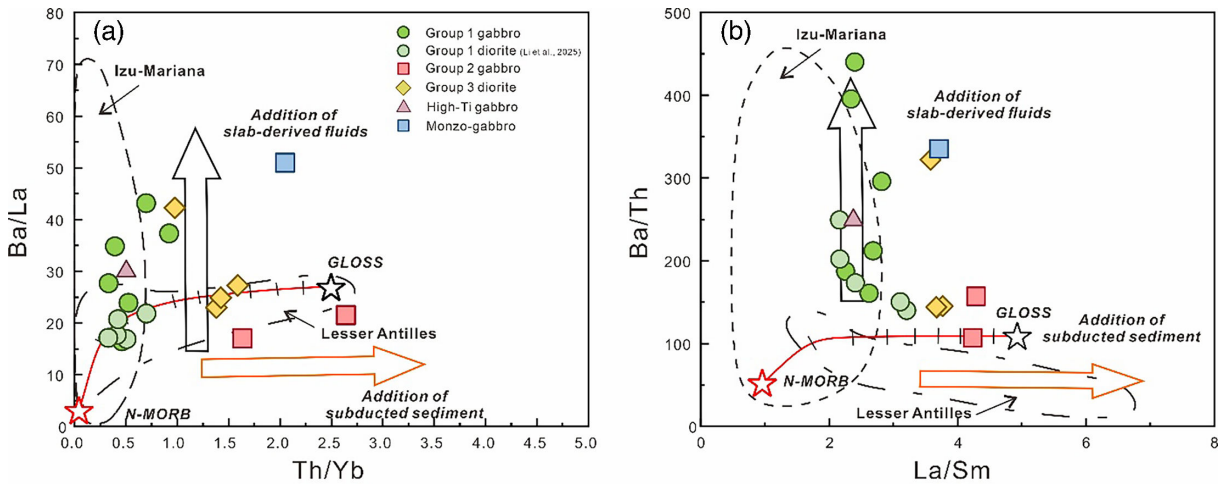

FIGURE 11: Th/Yb versus Ba/La (a) and La/Sm versus Ba/Th (b) diagrams illustrating the role of slab-derived hydrous fluids and subducted sediments on magma sources of Tianquan gabbro and diorite. Red line indicates mixing between N-MORB and global subducted sediment (GLOSS [141]). N-MORB is after [89].

of the La/Sm_N versus Sm/Yb_N systematics, as presented in [74], indicate that there are two clusters of Group 1 gabbros: one derived at high degrees of melting 5%–10% of a spinel-bearing lherzolite and the second formed at 6%–9% of melting of a garnet-bearing lherzolite (Figure 12(a)). The high-Ti gabbro formed at the highest degree of melting (10%) of a garnet-bearing lherzolite. Group 2 gabbros and the monzo-gabbro were derived from a garnet lherzolite as well, but at lower degrees, 1.8% and 2.2%, respectively. The melting curves in the Yb versus Nb/Yb diagram as presented in [75, 76] indicate that Group 1 gabbros were derived by 8%–18% melting of depleted harzburgite and 13%–16% melting of spinel lherzolite (Figure 12(b)). The high-Ti gabbro formed at 10% melting of harzburgite. Group 2 gabbros and monzo-gabbro were produced by, respectively, 7–9 and 2% melting of garnet lherzolite with 1% of garnet.

To explore relationships between Tianquan gabbros and diorites, we performed Rayleigh fractional crystallization modeling using the principles stated in [77] and most incompatible elements, such as REE and HFSE, in our case Nb and Y (Figure 12(c)). Such modeling has been used by many researchers studying old magmatic formations of orogenic belts worldwide [e.g. 78–82]. Of special value are ratios $(Nb/Y)_{PM}$ and $(Nb/Zr)_{PM}$ that mean an angle of a basic line in multi-element spectra of mafic rocks in respect to immobile elements. Such ratios allow evaluating a type of mantle source: depleted ($Nb/Y_{PM} < 1$) and undepleted ($Nb/Y_{PM} > 1$). Increased La/Sm_N, La/Nb_{PM}, and Th/Nb_{PM} serve as indicators of metasomatism-related source enrichments [e.g. 83, 84].

For our modeling, we chose the highest magnesian sample, gabbro TQ-23-14, as a source (online supplementary table S3). Starting concentrations in the source are shown in online supplementary table S8. According to the Harker diagrams, we admit that the main fractionating phases for the rock under study were olivine (Figures 7(a) and 7(b)) and clinopyroxene (Figures 7(a)–7(c)). Therefore, we chose these minerals for the modeling in a proportion of 1:1. Our modeling shows that the spectra of most Group 1 diorites are similar in shape to those of Group 1 gabbros (Figure 12(c)). All spectra have shapes similar to that of the model line, and all samples have close ratios of La/Sm_N and Nb/Y_{PM}: $La/Sm_{N(Gr1\ gabb)}$ =1.5–1.8, $Nb/Y_{PM(Gr1\ gabb)}$ = 0.7–1.2; $La/Sm_{N(Gr1\ dior)}$ =1.4–2.1, $Nb/Y_{PM(Gr1\ dior)}$ = 0.9–1.0. Note that Group 2 gabbros, the monzo-gabbro, and Group 3 diorites have higher Nb/Y_{PM} ($2.6_{av.}$, 6.3, and $1.6_{av.}$, respectively) suggesting more enriched sources. At relatively high degrees of fractionation of olivine and clinopyroxene from the starting source, we can obtain as high concentration of REE and HSFE as in Group 1 diorites. The results of the modeling confirm that Group 1 diorites were derived from Group 1 gabbros due to fractional crystallization.

5.2.3. Summary on Petrogenesis

Overall, the parental melts of all gabbroids and diorites were LREE enriched and experienced negligible fractionation of plagioclase ($Eu/Eu^* = 0.9–1.1$; Figures 8(a) and 8(c)). All such melts except for that of the monzo-gabbro underwent fractionation of olivine, clinopyroxene, and Fe-Ti oxides (Figures 7(a), 7(b), 7(e), 8(a), and 8(c)). Their parental melts were derived from isotopically depleted mantle wedge sources generated at subduction zones (Figures 9(a) and (b)). Subduction-related arc igneous rocks typically possess variable ratios of incompatible trace elements like Ba/La, Th/Yb, and Ba/Th reflecting the complex interaction of slab-derived fluids and mantle wedge melting. These ratios can be used to understand the source of the magmas and the processes involved in their formation [73, 85]. The isotope characteristics and the results of geochemical modeling suggest that the parental melts of Group 1 gabbro were derived by the relatively high degrees of melting (5%–10%) of depleted mantle wedge peridotite, harzburgite, or spinel lherzolite (Figures 12(a) and (b)), under the influence

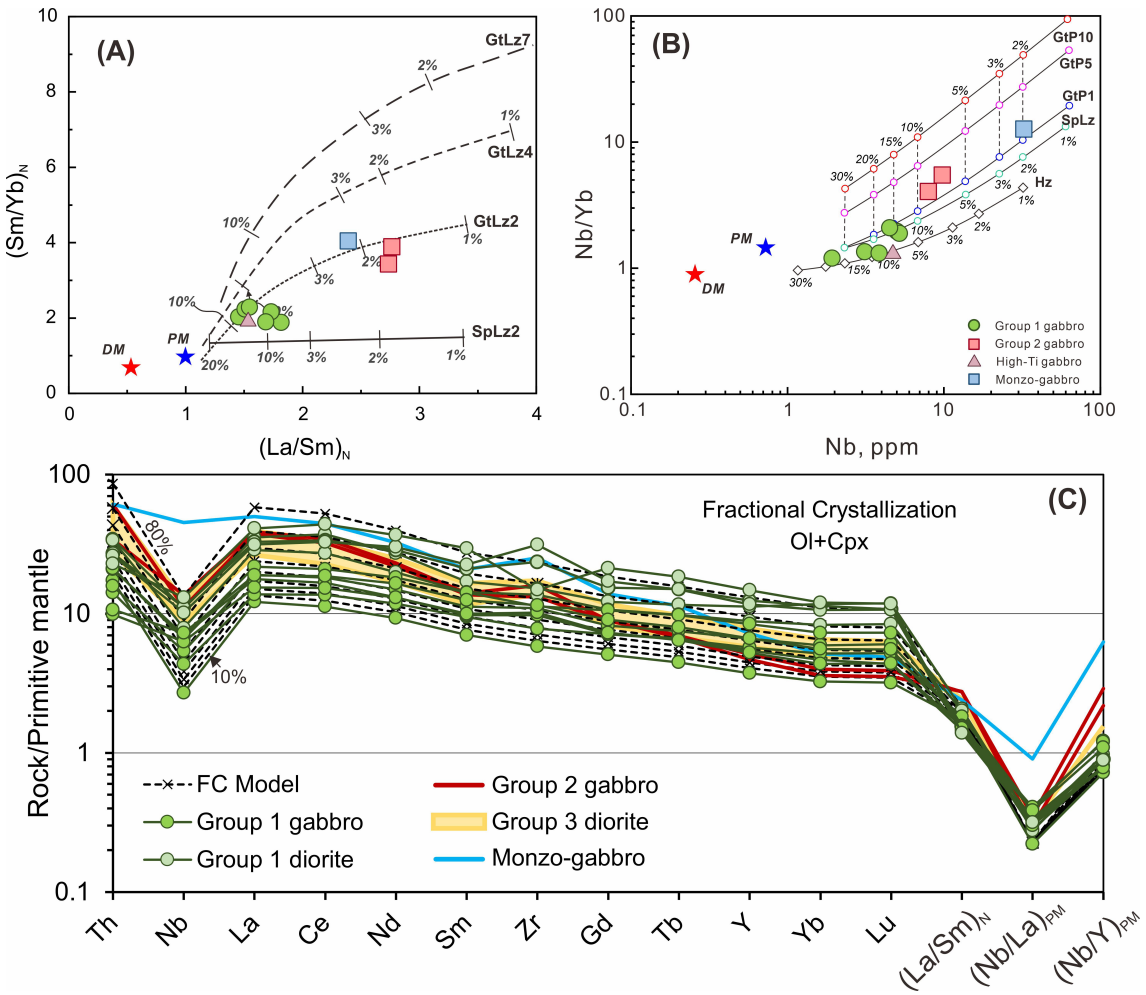

Figure 12: Geochemical modeling diagrams for Tianquan gabbros in comparison with melt compositions from nonmodal batch melting modeling. (a)$(Sm/Yb)_N$ versus $(La/Sm)_N$ after [73]. Dashed lines represent melting curves of a garnet-bearing lherzolite (GtLz) containing 2%, 4%, and 7% of garnet, and the solid line is the melting curve of lherzolite with 2% of spinel. (b) Nb versus Nb/Yb modeling based on partition coefficients from [142, 143]. The calculated melting curves are for spinel lherzolite (SpLz) and garnet peridotite containing 1%, 5%, and 10% of garnet (GtP). PM, primitive mantle; DM, depleted mantle. Numbers on curves refer to melting degrees after [144]. (c) a Rayleigh fractionation model illustrating fractional crystallization of a high-Mg Group 1 gabbro and derivation of Group 1 diorites.

of fluids separated from the subducted hydrated oceanic crust (Figures 9(c) and 11). Later, the melts experienced fractional crystallization of olivine and clinopyroxene to produce Group 1 gabbros.

Group 2 gabbro could be also formed by the melting of mantle wedge affected by both the fluids and the melts derived from the subducting oceanic slab, which would be more felsic and accordingly enriched in LREE. The interaction of such melts with the mantle peridotite would result in the replacement of olivine by clinopyroxene and, in presence of water, by amphibole and phlogopite [86]. Previous data from most of the 870–750 Ma mafic rocks of other localities of the western Yangtze Block also suggest a mantle wedge source affected by slab-derived fluids [8, 15, 28, 52].

Given that the LREE are less incompatible in clinopyroxene, amphibole, and mica compared to olivine [87], we would get a more LREE-enriched mantle source [88], like that produced Group 2 gabbros compared to Group 1 (Figure 11). Both groups of gabbro were derived from isotopically depleted mantle sources (Figures 9(a) and 9(b)), that, coupled with the Nb-Ta and Ti minimums in the spidergrams (Figure 8(b)), is typical of supra-subduction magmas. However, compared to Group 1 gabbros, Group 2 gabbros have higher REE (Figure 8(a)) and higher Th/Yb and La/Sm ratios implying a more significant addition of sediments to their parental melts (Figure 11). The increased contents of La and Nb result in a garnet-bearing source of Group 2 gabbros implying their formation at much lower degrees of melting of a garnet peridotite compared to Group 1 (Figure 12). However, their obvious supra-subduction origin allows us to suggest the higher involvement of sediment-derived fluids in their petrogenesis (Figure 11).

The high-Ti gabbro is a bit different from groups 1 and 2 gabbros as it actually resembles an alkaline gabbro (Figure 6(a)). It plots away from the trends in the Harker diagrams (Figure 7), has LREE higher than in Group 1 but lower than in Group 2 and the monzo-gabbro (Figures 8(a) and

8(b)), and therefore may be of different origin. However, the isotope characteristics of its mantle source (Figure 9) and the trace-element ratios (Figures 11 and 12) are similar to those of Group 1 gabbros. Although its REE pattern is similar to the modeled lines, we cannot link this sample with Group 1 because it is 15–25 Myr younger than those (Figures 5 and 13).

The geochemical features of the monzo-gabbro resemble those of intra-plate OIB-type basalts: LREE enriched (La/Yb_N = 9.7), HREE differentiated (Gd/Yb_N = 2.7); Nb-enriched (Figures 8(b) and 12(b)) [89–92]. The parental melt of the monzo-gabbro was derived through a low-degree melting of a geochemically enriched (Figure 8(a)), but isotopically depleted (Figures 9(a) and 9(b)) mantle source with a minimal interplay with subducted sediment-derived fluids and AOC-derived melts (Figures 8(b) and 12(b)). Probably, later its parental melt was affected by slab-derived fluids (Figure 11).

The Group 1 diorites formed by 60%–80% fractional crystallization of olivine and clinopyroxene (Figure 12(c)). The differentiating phases were the same melts that produced Group 1 gabbroids. Compared to Group 1 diorites, the Group 3 diorites show higher contents of SiO_2 and Al_2O_3 and total REE, but lower Fe_2O_3 (Figure 7). Note that their higher Nb/Y_{PM} average ratio (Figure 13) implies a mantle source different from that that produced Group 1 diorites (Figure 12(c)). The parental melts of Group 3 diorites could be also derived from an isotopically depleted mantle source (Figure 9(a)) that later interacted with subducted sediments (Figures 9(b) and 11).

To sum up, the magmatic rocks of the western Yangtze Block often display a continuous compositional evolution from mafic to intermediate and, finally, to felsic rocks, all derived from depleted mantle wedge sources with participation of slab-derived fluids and melts, and sediment-derived fluids. In addition to Tianquan gabbros, in western Yangtze, similar scenarios and conditions of petrogenesis have been reconstructed in the Nanba gabbroid complex [93], Guandaoshan and Tongde gabbro-diorite complexes [61, 62, 94, 95]. The geochemical and isotope variations in such gabbro-diorite complexes that are exposed at the western margin of the Yangtze Block suggest a successive differentiation of parental magmas in the lower-middle crust.

5.3. Tectonic Implications for Tianquan Magmatic Rocks and Tectonic Debates About Western Yangtze Magmatism

In the discrimination diagrams, Group 1 gabbros and diorites, Group 3 diorites, and the high-Ti gabbro plot in the fields of supra-subduction volcanic rocks, calc-alkaline or transitional to tholeiitic (Figure 14) that fits the classification diagrams (Figure 6). In addition, the Tianquan gabbros and diorites plot between the average compositions of magmatic rocks of world main arcs, intra-oceanic and continental, both tholeiitic and calc-alkaline. However, Group 2 gabbros plot away from Group 1 samples suggesting a mixed or more enriched magma source. The youngest monzo-gabbro takes a special position: it plots either in the field of intra-plate (continental rift) rocks or near those.

There have been a lot of debates on the tectonic settings of the emplacement of Neoproterozoic magmatic formations of the western Yangtze Block, most of which have been about the subduction-related versus rifting/mantle plume settings [1, 2, 6, 8, 10, 11, 13, 96]. Researchers have been arguing for continuous variably differentiated mafic to felsic series or bimodal magmatic series. To resolve such a controversy is critical to understand the tectonic evolution of the whole SCC as well as the position of South China in Rodinia [12, 35, 36]. Note that both competing models are based on various data, in particular, geochronological and isotope-geochemical data, from Neoproterozoic magmatic rocks exposed around the Yangtze Block.

In general, the Neoproterozoic magmatism of western Yangtze was active at 860–850 and 830–740 Ma [10] (Figures 1 and 2, section 5.1), although there are single U-Pb zircon ages between 850 and 830 Ma, such as the Pengguan granite (844 ± 6 Ma; [18]), Shimian diabase (837 ± 8 Ma; [58]), and Yonglang granite (840 ± 2 Ma; [60]). The older episode of magmatism was interpreted to be linked with the Jiangnan (or Sibao) orogeny triggered by the amalgamation of the Cathaysia and Yangtze blocks. An extensional anorogenic setting was proposed for the younger magmatic rocks, and their initiation was attributed to a mantle plume [6, 10, 12, 97]. The mantle plume model implies the collision between the Yangtze and Cathaysia blocks and formation of the South China continent at around 900 Ma, that is during the Grenvillian orogeny [98, 99], and the arrival of a mantle plume to initiate intra-continental rifting at ca. 825 Ma [6, 12, 100]. However, recent geochronological data from clastic rocks indicate that the syn-orogenic strata of the Jiangnan orogen formed at ca. 860–820 Ma thus excluding the rifting at 825 Ma [53, 101, 102]. In addition, volcanic rocks (basalt to rhyolite) interbedded with early Neoproterozoic clastic rocks (sandstone, tuffaceous sandstone, siltstone) yielded zircon ages of ca. 830 Ma [54, 103–106] suggesting an earlier assembly of the Yangtze and Cathaysia blocks at ca. 830 Ma or even younger. The overall duration of the Neoproterozoic magmatism at the western margin of the Yangtze Block took a rather long time from 890 Ma to 740 Ma [11 and references therein], that is uncommon for mantle plume magmatism typically characterized by short but greatly voluminous volcanic eruptions [e.g. 107–110]. Finally, the Neoproterozoic magmatic formations of the western Yangtze Block are dominated by diorites, granodiorites, and granites as batholiths and stocks (Figures 1 and 2; [11]), whereas plume-related rocks are typically mafic flood basalts, lava flows, and dykes [e.g. 91, 107, 111, 112].The Neoproterozoic magmatic rocks

An early argument for the mantle plume model was the scarcity or absence of intermediate rocks in the western Yangtze Block, for example, in the compositionally bimodal volcanic series of the Suxiong Fm [5, 36], compared to the widespread exposures of mafic and felsic rocks. However, later there have been obtained more data from magmatic rocks showing more and more localities of intermediate

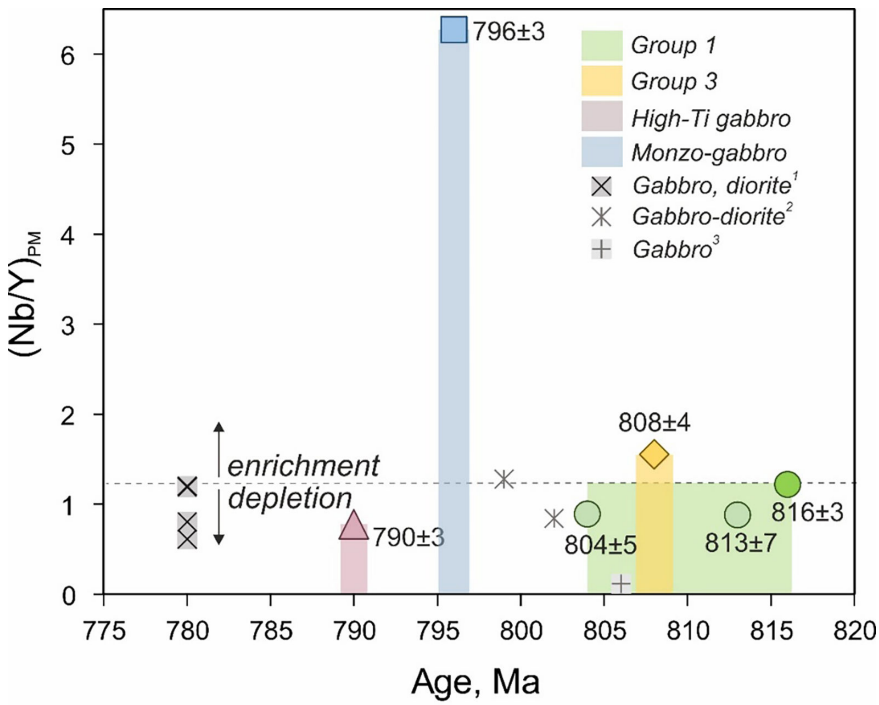

FIGURE 13: U-Pb zircon ages versus $(Nb/Y)_{PM}$ diagram illustrating different mantle sources of Tianquan rocks at different time periods in comparison with gabbros and diorites of 1-Luding [140], 2-Baoxing [57], and 3-Shimian [25] complexes of the central part of western Yangtze.

rocks, first of all, diorites: ca. 858 Ma Tongde diorite [94], 856 Ma Guandaoshan gabbro-diorite and quartz diorite [61], 830 Ma Tongde dioritic dyke [26], 810 Ma Tianquan diorites (this paper), and other localities [e.g. 2, 27, 55, 93]. Therefore, a large body of evidence argues against the mantle plume as a trigger of Neoproterozoic magmatism along the western Yangtze Block.

The alternative hypothesis implies an early Neoproterozoic subduction system at the western margin of the Yangtze Block at 860–740 Ma to form the Panxi-Hannan Arc [11, 50, 113, 114]. In this study, we have found that the Neoproterozoic Tianquan magmatic rocks mostly consist of normal gabbro-diorites (816, 804 Ma) that display typical trace-element signatures of subduction-related igneous rocks: variable degrees of depletions in HFSEs and enrichments in LREE and LILEs. In the Hf-Th-Ta, Y-La-Nb, and Nb-Zr-Y diagrams (Figure 14), they are mainly plotted within the volcanic arc field suggesting an island arc tectonic setting. Thus, the newly identified Tianquan magmatic rocks provide a robust evidence for existence of a supra-subduction zone system along the western Yangtze Block in mid-Neoproterozoic time.

Another evidence for the long-lived supra-subduction zone system comes from Neoproterozoic mafic to intermediate rocks, I-type arc granitoids, and adakites that are also abundant in western Yangtze. There have been obtained plenty of data confirming that mafic to intermediate rocks were derived from mantle wedge melts affected by slab-derived fluids, sediment melts, or melts from AOC [e.g. 15, 27, 93]. In addition, it has been estimated that the associated granitoids and adakites formed by partial melting of juvenile thickened lower crust or by melting of subducted oceanic crust in the presence of fluids and emplaced in a supra-subduction setting [8, 41, 53, 115, 116; this paper].

In the Tianquan County, we identified a younger monzo-gabbro (796 Ma) that possesses an OIB geochemical affinity. In western Yangtze, there are other occurrences of such alkaline mafic rocks displaying typical compositions of within-plate basalts, that is enriched in Ti, Nb, and LREE and having differentiated HREE (Figures 7(g)–7(h), 8, and 14(b)-14(c)) that formed at 810–790 Ma [35, 117–119] and may indicate a rifting setting. A group of authors has suggested a back-arc extension setting due to long-lived eastward subduction of oceanic slab [103]. The subduction to back-arc extension model also explains the presence of Neoproterozoic sedimentary and volcano-sedimentary strata along the western Yangtze Block deposited at an active continental margin. The strata are attributed to the Xixiang, Bikou, and Yanbian groups, and they are exposed over a huge area from north to south in western Yangtze. The sedimentary sequences are dominated by first-cycle flysch-type sedimentary clastic rocks interbedded with volcanogenic rocks [29, 30, 32, 63, 97, 120]. A detailed study of the sandstones of the Yanbian Group including petrography and U-Pb ages of detrital zircons has shown that those clastic rocks were derived by destruction of an island arc and were deposited in a back-arc basin at ca. 860 ca [30, 32]. More evidence for the back-arc extension comes from ca. 800 Ma bimodal volcanics of the Suxiong Fm. exposed in the Kangdian region of western Yangtze. Therefore, the combined evidence suggests the continuous eastward subduction of an oceanic slab beneath western

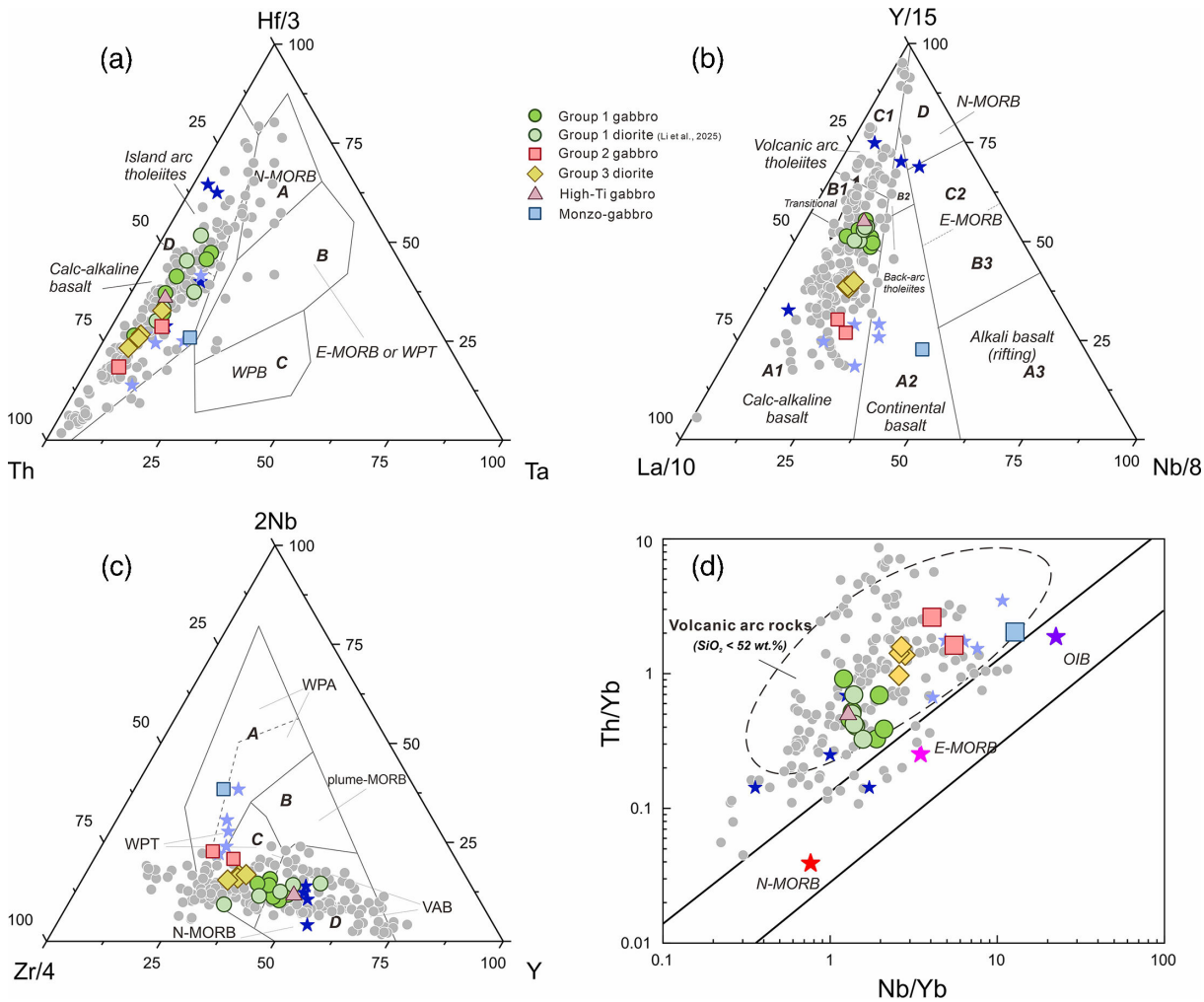

FIGURE 14: Tectonic discrimination ternary diagrams for Tianquan gabbro and diorites: (a) Th-Hf/3-Ta [145]; (b) La/10-Y/15-Nb/8 [146]; (c) Zr/4-2Nb-Y [147]; (d), Nb/Yb versus Th/Yb [148]. N-MORB, normal midocean ridge basalt; E-MORB, enriched midocean ridge basalt; OIB, oceanic island basalt; WPT/B, within plate tholeiite/basalt; VAB, volcanic arc basalt; WPA, within-plate alkali basalt. Light gray circles are for the Neoproterozoic gabbros and diorites of the western Yangtze Block (online supplementary table S9) and arc basalts are from [73]. The field outlined by dashed line in D is for arc volcanic rocks with SiO_2 < 52 wt.% from the GEOROC database (https://georoc.eu/georoc/).

Yangtze Block during early Neoproterozoic time (Tonian). That time the Yangtze and Cathaysia blocks took exterior positions in the configuration of Rodinia, possibly at its northwestern margin (Figure 15; [121]).

The continuous trends from gabbro (Group 1) to diorites (Figures 6(a), 6(b), and 7) and their geochemical characteristics typical of supra-subduction magmas (enriched LREEs, depleted HSFEs; Figure 8) support rather the subduction zone model implying a continuous magmatism (at least from 816 to 809 Ma) and fractional crystallization, than the mantle plume model implying bimodal magmatism. However, we can assume an episode of continental margin rifting magmatism as the youngest monzo-gabbro plots in the field of continental rifting basalt (Figure 14(b)). Thus, the new localities of diorite, this time from Tianquan (Figure 2), provide more evidence against the model of Neoproterozoic bimodal mantle plume magmatism, but in favor of the supra-subduction magmatism though followed by continental margin rifting.

According to the Lu-Hf and Sm-Nd isotope systematics, the Tianquan supra-subduction magmatic rocks were derived from depleted mantle sources (Figures 9(a) and 9(b)) though with participation of slab- derived fluids (Figure 9(c)). These geochemical and isotope characteristics suggest rather an island-arc origin of the Tianquan subduction-related gabbro than an active continental margin. More evidence for such an intra-oceanic arc and adjacent fore-arc and back-arc basins comes, respectively, from the supra-subduction volcanic rocks of the Suxiong Fm. formed at 800–780 Ma [37, 122] and from the clastic rocks (greywacke sandstones) of the Hengdan Group in the northern Yangtze Block with U-Pb detrital zircon age peaks at 780 Ma and 760 Ma [120, 123].

Another intra-oceanic arc, the Bikou arc, was proposed for the NW Yangtze [124], but for the western Yangtze

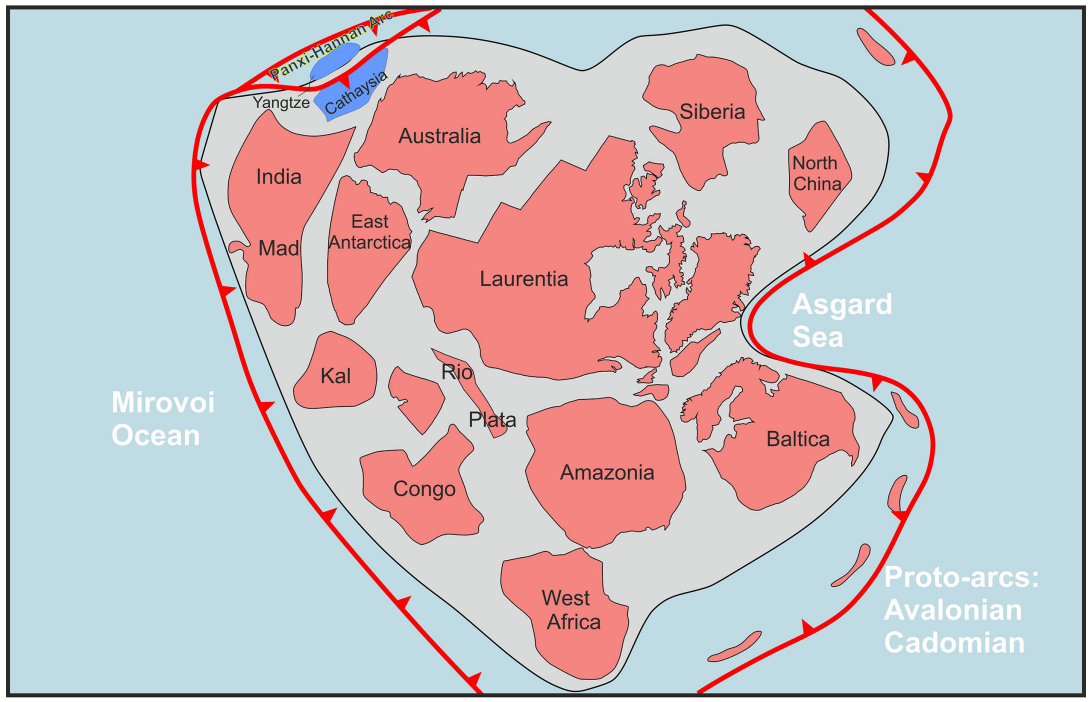

Figure 15: The ca. 900 Ma paleogeographic position of the Yangtze Block in Rodinia [121].

Block, most scholars have been discussing rather an active continental margin arc or Japan-type intra-oceanic arc [15, 29, 31, 32, 93]. However, we argue that in such a setting (continental arc), the magmatic melts would be derived from more enriched mantle sources with recycled or mixed isotope characteristics like the magmatic rocks of SW Japan [e.g. 125–131]. In the modern western Pacific, the SW Japan-Ryukyu-Taiwan magmatism and Izu-Bonin-Mariana magmatism represent a "couple" of adjacent coeval peri-continental and intra-oceanic arc systems, respectively, with a very small back-arc basin in the north and a huge one in the south (Figure 16; online supplementary table S9 and S10). Therefore, we suggest that a similar setting could exist at the western active margin of the Yangtze Block in late Tonian time and that the Tianquan arc was a southern extension of the Bikou arc [124].

6. CONCLUSIONS

The first U-Pb zircon ages, whole-rock geochemical, and Nd isotope data and Hf-in-zircon isotope data from gabbros and gabbro-diorites and the new data from diorites of the Tianquan County in western Sichuan, and diorites, confirmed the compositionally variable character of the Neoproterozoic magmatism at the western margin of the Yangtze Block. The dataset under study includes mafic (gabbro) to intermediate (diorite) rocks. There are several geochemically distinct groups of rocks: Group 1 gabbro and diorites (normal), Group 2 gabbros (REE enriched), Group 3 diorites (high Al-K), high-Ti gabbro, and monzo-gabbro. The ages of Tianquan gabbros (816 Ma) match the 830–810 and 800–790 Ma peaks of magmatism in the western Yangtze Block, and the ages of Tianquan diorites fit the 810–800 Ma peak. Group 1 gabbro is less enriched in light REE and has less differentiated heavy REE (La/Yb_N = 2.9–3.7; La/Sm_N = 1.5–1.8; Gd/Yb_N = 1.4–1.6) compared to Group 2 gabbros (La/Yb_N = 9.4–10.8; La/Sm_N = 2.7–2.8, Gd/Yb_N = 2.2–2.5), monzo-gabbro (796 Ma) and high-Ti gabbro (790 Ma). All rocks are characterized by positive $\varepsilon Nd(t)$ (+1.9 to +6.0) and $\varepsilon Hf(t)$ (+9.2 to +17.8). Group 1 gabbros (816 Ma) were derived by high-degree partial melting of depleted harzburgite and spinel lherzolite with participation of subduction-related fluids and then experienced 10%–80% fractionation of olivine and clinopyroxene to produce Group 1 diorites (813 and 804 Ma). Group 2 gabbros were derived by low-degree melting of a more enriched mantle source affected by slab-derived melts. Group 3 diorites (808 Ma), compared to Group 1 diorites, have lower contents of REE, lowest $\varepsilon Nd(t)$ (+1.9), and large involvement of subducted sediments in their petrogenesis; they formed from a different source. The monzo-gabbro (796 Ma) is compositionally similar to OIB-type intra-plate lavas; its parental melt was derived by a low-degree melting of a garnet lherzolite. The youngest high-Ti gabbro (790 Ma) formed at conditions of petrogenesis similar to those of Group 1 gabbros, but their much younger age and the results of trace-element modeling do not allow us to consider them as a single magmatic series. All rocks except for the monzo-gabbro possess supra-subduction geochemical features and were possibly emplaced in a setting of intra-oceanic island arc. The monzo-gabbro was possibly emplaced in a rifting setting. Overall, our data confirm that the Neoproterozoic (Tonian) magmatism at the western active margin of the Yangtze Block was mostly related to oceanic subduction and was developing

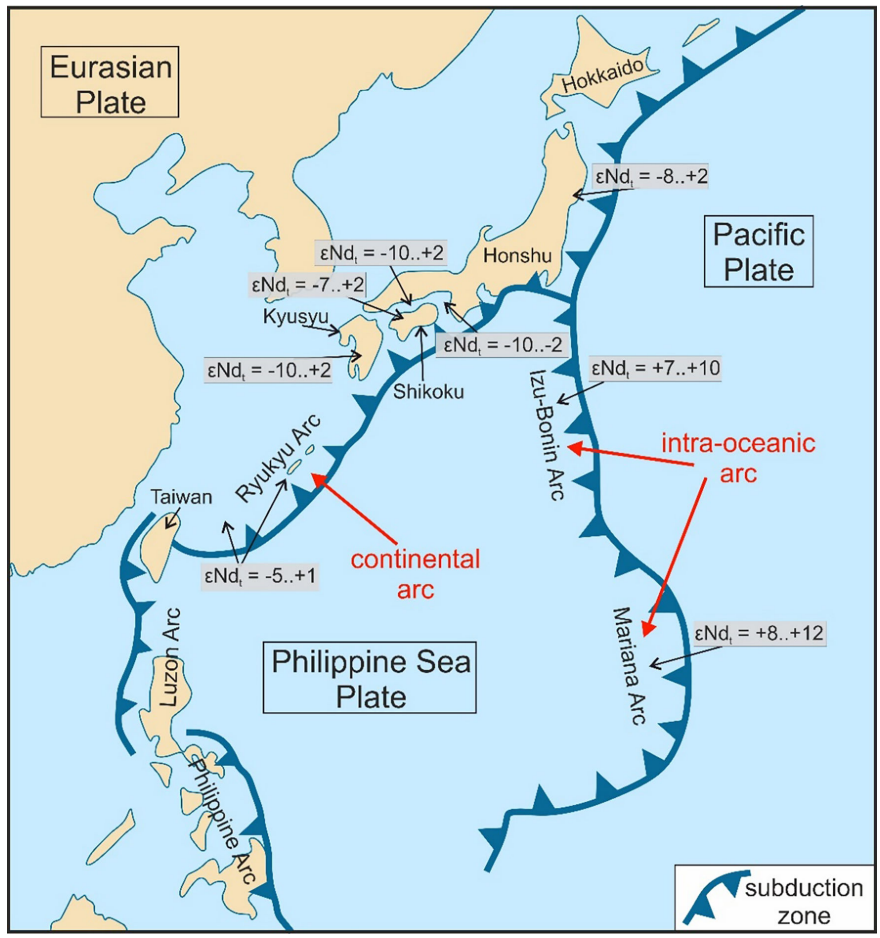

FIGURE 16: A review figure illustrating main Nd isotope characteristics of arc magmatic complexes of SW Japan, Ryukyu-Taiwan, and Izu-Bonin-Mariana arc systems. Data sources: [49, 125–127, 129–131, 149–155] (for details see online supplementary table S10).

continuously in space (north to south) and time (ca. 860–800 Ma). The 860–800 stage of supra-subduction magmatism (Groups 1–3) was followed by a stage of back-arc rifting at ca. 796 Ma (monzo-gabbro) and possible initiation of a new subduction zone at ca. 790 Ma (high-Ti gabbro).

Data Availability

The data for this study are available in supplementary material.

Conflicts of Interest

The authors declare that they have no conflicts of interest.

Funding Statement

This study was financially supported by the Fundamental Research Funds for the Central Universities [grant numbers 2682024CX080 and 2582025CX156)], State Bureau of Foreign Experts Affairs [grant number Y20240079], National Natural Science Foundation of China [grant number W2431031], Special Funding for Sichuan Postdoctoral Science Foundation, and the Ministry of Science and Higher Education of Russia, State Assignment Projects [grant numbers 122041400044-2 and FSUS-2020-0039].

Acknowledgments

We appreciate very much the organizational support from Prof. Zhao Xiaoyan and Dr. Liao Xin, both from the Faculty of Geoscience and Engineering (FGSE) of SWJTU. We also extend our cordial thanks to Prof. Zou Hao from the Chengdu University of Technology and his students and to FGSE SWJTU students Lv Yudong, Ma Xiaoyang, and Cao Yiming for assistance during the fieldwork.

Supplementary Materials

TABLE S1:

Supplementary Materials

Supplementary Material 1:

Supplementary Materials

FIGURE S1:

Supplementary Materials

FIGURE S2:

Supplementary Materials

FIGURE S3:

Supplementary Materials

FIGURE S4:

Supplementary Materials

FIGURE S5:

References

[1] G. C. Zhao and P. A. Cawood, "Tectonothermal evolution of the Mayuan assemblage in the Cathaysia Block; Implications for neoproterozoic collision-related assembly of the South China craton", *American Journal of Science*, vol. 299, no. 4, pp. 309–339, 1999.

[2] Y. Dong, X. Liu, M. Santosh, et al., "Neoproterozoic accretionary tectonics along the Northwestern margin of the Yangtze Block, China: Constraints from zircon U–Pb geochronology and geochemistry", *Precambrian Research*, vol. 196–197, pp. 247–274, 2012.

[3] P. A. Cawood, Y. J. Wang, Y. J. Xu, et al, "Locating South China in Rodinia and Gondwana: A fragment of greater India lithosphere", *Precambrian Research*, vol. 103, no. 1–2, pp. 55–88, 2013.

[4] H. Zou, H. Li, Z. Li, et al., "Integrated detrital rutile and detrital zircon ages: A new perspective on the tectonic evolution of South China", *National Science Review*, vol. 11, no. 12, 2024.

[5] Z.-X. Li, X. Li, H. Zhou, and P. D. Kinny, "Grenvillian continental collision in South China: New SHRIMP U-Pb zircon results and implications for the configuration of Rodinia", *Geology*, vol. 30, no. 2, 2002.

[6] Z. X. Li, X. H. Li, and P. D. Kinny, "Geochronology of neoproterozoic syn-rift magmatism in the Yangtze Craton, South China and correlations with other continents: Evidence for a mantle superplume that broke up Rodinia", *Precambrian Research*, vol. 122, no. 1–4, pp. 85–109, 2003.

[7] M. Zhou, A. K. Kennedy, M. Sun, J. Malpas, and C. M. Lesher, "Neoproterozoic arc-related mafic intrusions along the northern margin of South China: Implications for the accretion of Rodinia", *The Journal of Geology*, vol. 110, no. 5, pp. 611–618, 2002.

[8] M. Zhou, Y. Ma, D. Yan, X. Xia, J. Zhao, and M. Sun, "The Yanbian terrane (southern Sichuan province, SW China): A neoproterozoic arc assemblage in the western margin of the Yangtze block", *Precambrian Research*, vol. 144, no. 1–2, pp. 19–38, 2006.

[9] L. Xianhua, L. Zhengxiang, Z. Hanwen, L. Ying, L. Xirong, and L. Wuxian, "SHRIMP U-Pb zircon age, geochemistry and Nd isotope of the Guandaoshan pluton in SW Sichuan: Petrogenesis and tectonic significance", *Science in China Series D Earth Sciences*, vol. 46, no. S1, pp. 73–83, 2003.

[10] X.-H. Li, Z.-X. Li, J. A. Sinclair, W.-X. Li, and G. Carter, "Revisiting the 'Yanbian terrane': Implications for neoproterozoic tectonic evolution of the western Yangtze block, South China", *Precambrian Research*, vol. 151, no. 1–2, pp. 14–30, 2006.

[11] J.-H. Zhao, Q.-W. Li, H. Liu, and W. Wang, "Neoproterozoic magmatism in the western and northern margins of the Yangtze block (South China) controlled by slab subduction and subduction-transform-edge-propagator", *Earth-Science Reviews*, vol. 187, pp. 1–18, 2018.

[12] Z. X. Li, X. H. Li, P. D. Kinny, and J. Wang, "The breakup of Rodinia: Did it start with a mantle plume beneath South China?", *Earth and Planetary Science Letters*, vol. 173, no. 3, pp. 171–181, 1999.

[13] X. H. Li, Z. X. Li, and W. C. Ge, "Neoproterozoic granitoids in South China: Crustal melting above a mantle plume at ca. 825 ma?", *Precambrian Research*, vol. 122, no. 1–4, pp. 45–83, 2003.

[14] G. C. Zhao and P. A. Cawood, "Precambrian geology of China", *Precambrian Research*, vol. 222–223, pp. 13–54, 2012.

[15] J.-H. Zhao, M.-F. Zhou, Y.-B. Wu, J.-P. Zheng, and W. Wang, "Coupled evolution of neoproterozoic arc mafic magmatism and mantle wedge in the western margin of the South China craton", *Contributions to Mineralogy and Petrology*, vol. 174, no. 4, pp. 1–16, 2019.

[16] G. W. Zhang, Y. P. Dong, and S. C. Lai, "Mianlü tectonic zone and mianlü suture zone on southern margin of Qinling-Dabie orogenic belt"ee, *Science in China Series D*, vol. 47, no. 4, p. 300, 2004.

[17] Z. Xue, W. Lin, Y. Chu, W. Wei, Z. Feng, and J. Zhang, "Late triassic successive amalgamation between the South China and North China blocks: Insights from structural analysis and magnetic fabrics study of the Bikou terrane and its adjacent area, northwestern Yangtze Block, Central China", *GSA Bulletin*, vol. 134, no. 7–8, pp. 2051–2071, 2022.

[18] D. Yan, M. Zhou, G. Wei, et al., "The pengguan tectonic dome of Longmen mountains, Sichuan province: Mesozoic denudation of a neoproterozoic magmatic arc-basin system", *Science in China Series D*, vol. 51, no. 11, pp. 1545–1559, 2008.

[19] D. Yan, M. Zhou, G. Wei, et al., "Collapse of Songpan-Garzê Orogenic belt resulted from mesozoic middle-crustal ductile channel flow: Evidences from deformation and metamorphism within Sinian-paleozoic strata in hinterland of longmenshan foreland thrust belt", *Earth Science Frontiers*, vol. 15, no. 3, pp. 186–198, 2008.

[20] P. A. Cawood, G. Zhao, J. Yao, W. Wang, Y. Xu, and Y. Wang, "Reconstructing South China in phanerozoic and precambrian supercontinents", *Earth-Science Reviews*, vol. 186, pp. 173–194, 2018.

[21] G. C. Zhao, "Jiangnan Orogen in South China: Developing from divergent double subduction", *Gondwana Research*, vol. 27, no. 3, pp. 1173–1180, 2015.

[22] L. Shu, J. Yao, B. Wang, M. Faure, J. Charvet, and Y. Chen, "Neoproterozoic plate tectonic process and phanerozoic geodynamic evolution of the South China block", *Earth-Science Reviews*, vol. 216, p. 103596, 2021.

[23] Q. Chen, M. Sun, G. Zhao, et al., "Episodic crustal growth and reworking of the Yudongzi terrane, South China: Constraints from the archean ttgs and potassic granites and paleoproterozoic amphibolites", *Lithos*, vol. 326–327, pp. 1–18, 2019.

[24] M. R. Greentree, Z.-X. Li, X.-H. Li, and H. Wu, "Late mesoproterozoic to earliest neoproterozoic basin record of the Sibao orogenesis in western South China and relationship to the assembly of Rodinia", *Precambrian Research*, vol. 151, no. 1–2, pp. 79–100, 2006.

[25] J.-H. Zhao, P. D. Asimow, M.-F. Zhou, J. Zhang, D.-P. Yan, and J.-P. Zheng, "An andean-type arc system in Rodinia constrained by the neoproterozoic Shimian ophiolite in South China", *Precambrian Research*, vol. 296, pp. 93–111, 2017.

[26] Q. W. Li and J. H. Zhao, "The neoproterozoic high-Mg dioritic dikes in South China formed by high pressures fractional crystallization of hydrous basaltic melts", *Precambrian Research*, vol. 309, pp. 198–211, 2018.

[27] Y. Zhu, S. Lai, J. Qin, et al., "Genesis of ca. 850–835 ma high-Mg# diorites in the western Yangtze Block, South China: Implications for mantle metasomatism under the subduction process", *Precambrian Research*, vol. 343, 2020.

[28] F. Xiong, Q. Liu, M. Hou, and S. Yan, "Petrogenesis of neoproterozoic mafic dykes in western Yangtze Block, South China: Implications for the assembly and break-up of Rodinia", *International Geology Review*, vol. 65, no. 14, pp. 2191–2211, 2023.

[29] W. H. Sun, M. F. Zhou, and J. H. Zhao, "Geochemistry and tectonic significance of basaltic lavas in the neoproterozoic Yanbian group, southern Sichuan province, Southwest China", *International Geology Review*, vol. 49, no. 6, pp. 554–571, 2007.

[30] W. Sun, M. Zhou, D. Yan, J. Li, and Y. Ma, "Provenance and tectonic setting of the neoproterozoic Yanbian group, western Yangtze Block (SW China)", *Precambrian Research*, vol. 167, no. 1–2, pp. 213–236, 2008.

[31] Y. A. N. Quanren, W. Zongqi, A. D. Hanson, et al, "SHRIMP age and geochemistry of the Bikou volcanic terrane: Implications for neoproterozoic tectonics on the northern margin of the Yangtze craton", *Acta Geologica Sinica - English Edition*, vol. 77, no. 4, pp. 479–490, 2003.

[32] Q. yan, A. D. Hanson, Z. Wang, et al., "Neoproterozoic subduction and rifting on the northern margin of the Yangtze plate, China: Implications for rodinia reconstruction", *International Geology Review*, vol. 46, no. 9, pp. 817–832, 2004.

[33] L. Q. Xia, Z. C. Xia, X. Y. Xu, et al, "Petrogenesis of the bikou group volcanic rocks(In Chinese)", Earth Science Frontiers, vol. 14, no. 3, pp. 84–101, 2007.

[34] X.-C. Wang, X.-H. Li, W.-X. Li, et al., "The bikou basalts in the northwestern Yangtze block, South China: Remnants of 820-810 ma continental flood basalts?", *Geological Society of America Bulletin*, vol. 120, no. 11–12, pp. 1478–1492, 2008.

[35] X. Li, Z.-X. Li, H. Zhou, Y. Liu, and P. D. Kinny, "U–Pb zircon geochronology, geochemistry and Nd isotopic study of neoproterozoic bimodal volcanic rocks in the Kangdian rift of South China: Implications for the initial rifting of Rodinia", *Precambrian Research*, vol. 113, no. 1–2, pp. 135–154, 2002.

[36] X. H. Li, C. S. Qi, and Y. Liu, "Petrogenesis of the neoproterozoic bimodal volcanic rocks along the western margin of the Yangtze block: New constraints from Hf isotopes and Fe/Mn ratios", *Chinese Science Bulletin*, vol. 50, no. 21, 2005.

[37] J. W. Zhuo, Z. F. Jiang, X. S. Jiang, et al, "SHRIMP zircon U-Pb ages for the stereotype section of neoproterozoic suxiong formation in western Sichuan province and their geological significance", *In Chinese*, vol. 63, no. 1, pp. 177–188, 2017.

[38] J. W. Zhuo, X. S. Jiang, J. Wang, et al, "Zircon SHRIMP U-Pb age of sedimentary tuff at the bottom of neoproterozoic kaijianqiao formation in western Sichuan, and its geological implication(in Chinese)", *Journal of Mineralogy and Petrology*, vol. 35, no. 1, pp. 91–99, 2015.

[39] K. R. Fu, "Dating of the key formations, sedimentary geological characteristics and the tectonic significance of rift filling sequence in Kangdian rift(In Chinese)", China University of Geoscience, 2020.

[40] Q. R. Meng, E. Wang, and J. M. Hu, "Mesozoic sedimentary evolution of the Northwest Sichuan Basin: Implication for continued clockwise rotation of the South China Block", *Geological Society of America Bulletin*, vol. 117, no. 3, 2005.

[41] F. Xiong, H. Zhong, H. Huang, X. Liu, and M. Hou, "Petrogenetic and tectonic implications of neoproterozoic igneous rocks from the western Yangtze block, South China", *Precambrian Research*, vol. 387, 2023.

[42] Sichuan Provincial Bureau of Geology and Mineral Resources (SPBGMR), Regional geology of Sichuan province(in Chinese), Geological Publishing House, Beijing, 1991.

[43] S. W. Liu, K. Yang, Q. G. Li, et al, "Petrogenesis of the neoproterozoic baoxing complex and its constraint on the tectonic environment in western margin of Yangtze craton(In Chinese)", Earth Science Frontiers, vol. 16, no. 2, pp. 108–117, 2009.

[44] Y. B. Li, X. Ren, I. Safonova, et al, "Early neoproterozoic oceanic subduction along the western Yangtze Block: Constraints from genesis of Tianquan diorites in the western Sichuan(In Chinese)", Journal of Chengdu University of Technology (Science & Technology Edition), vol. 52, no. 3, pp. 1–22, 2025.

[45] L. M. Heaman, R. Bowins, and J. Crocket, "The chemical composition of igneous zircon suites: Implications for geochemical tracer studies", *Geochimica et Cosmochimica Acta*, vol. 54, no. 6, pp. 1597–1607, 1990.

[46] P. W. O. Hoskin and U. Schaltegger, "The composition of zircon and igneous and metamorphic petrogenesis", *Reviews in Mineralogy and Geochemistry*, vol. 53, no. 1, pp. 27–62, 2003.

[47] A. I. S. Kemp, C. J. Hawkesworth, G. L. Foster, et al., "Magmatic and crustal differentiation history of granitic rocks from Hf-O isotopes in zircon", *Science (New York, N.Y.)*, vol. 315, no. 5814, pp. 980–983, 2007.

[48] W. J. Collins, E. A. Belousova, A. I. S. Kemp, and J. B. Murphy, "Two contrasting phanerozoic orogenic systems revealed by Hafnium isotope data", *Nature Geoscience*, vol. 4, no. 5, pp. 333–337, 2011.

[49] S. M. Straub, S. L. Goldstein, C. Class, A. Schmidt, and A. Gomez-Tuena, "Slab and mantle controls on the Sr–Nd–Pb–Hf isotope evolution of the post 42 ma izu–bonin volcanic arc", *Journal of Petrology*, vol. 51, no. 5, pp. 993–1026, 2010.

[50] Y. Dong, X. Liu, M. Santosh, et al., "Neoproterozoic subduction tectonics of the northwestern Yangtze Block in South China: Constrains from zircon U–Pb geochronology and geochemistry of mafic intrusions in the hannan massif", *Precambrian Research*, vol. 189, no. 1–2, pp. 66–90, 2011.

[51] J.-H. Zhao, M.-F. Zhou, J.-P. Zheng, and S.-M. Fang, "Neoproterozoic crustal growth and reworking of the northwestern Yangtze Block: Constraints from the Xixiang dioritic intrusion, South China", *Lithos*, vol. 120, nos. 3–4, pp. 439–452, 2010.

[52] J. H. Zhao and M. F. Zhou, "Geochemistry of neoproterozoic mafic intrusions in the Panzhihua district (Sichuan province, SW China): Implications for subduction-related metasomatism in the upper mantle", *Precambrian Research*, vol. 152, no. 1–2, pp. 27–47, 2007.

[53] J. H. Zhao and M. F. Zhou, "Secular evolution of the neoproterozoic lithospheric mantle underneath the northern margin of the Yangtze block, South China", *Lithos*, vol. 107, no. 3–4, pp. 152–168, 2009.

[54] W. Wang, M.-F. Zhou, J.-H. Zhao, M. K. Pandit, J.-P. Zheng, and Z.-R. Liu, "Neoproterozoic active continental margin in the southeastern Yangtze block of South China: evidence from the ca. 830–810ma sedimentary strata", *Sedimentary Geology*, vol. 342, pp. 254–267, 2016.

[55] B. Luo, R. Liu, H. Zhang, et al., "Neoproterozoic continental back-arc rift development in the northwestern Yangtze block: Evidence from the hannan intrusive magmatism", *Gondwana Research*, vol. 59, pp. 27–42, 2018.

[56] L. Xiao, H.-F. Zhang, P.-Z. Ni, H. Xiang, and X.-M. Liu, "LA-ICP-MS U–Pb zircon geochronology of early neoproterozoic mafic-intermediat intrusions from NW margin of the Yangtze block, South China: Implication for tectonic evolution", *Precambrian Research*, vol. 154, no. 3–4, pp. 221–235, 2007.

[57] E. Meng, F.-L. Liu, L.-L. Du, P.-H. Liu, and J.-H. Liu, "Petrogenesis and tectonic significance of the baoxing granitic and mafic intrusions, southwestern China: Evidence from zircon U–Pb dating and Lu–Hf isotopes, and whole-rock geochemistry", *Gondwana Research*, vol. 28, no. 2, pp. 800–815, 2015.

[58] P. Hu, Q. Zhai, J. Wang, et al., "U–Pb zircon geochronology, geochemistry, and Sr–Nd–Hf–O isotopic study of middle neoproterozoic magmatic rocks in the Kangdian rift, South China: Slab rollback and backarc extension at the northwestern edge of the Rodinia", *Precambrian Research*, vol. 347, 2020.

[59] J. Zhang, Y. Liu, X. Ding, P. Liu, C. Shi, and H. Zhang, "Subduction retreating caused the external breakup of Rodinia: Constraints from the neoproterozoic igneous rocks in the western Yangtze block, South China", *Journal of Asian Earth Sciences*, vol. 271, p. 106229, 2024.

[60] Y. Zhu, S. Lai, J. Qin, et al., "Neoproterozoic metasomatized mantle beneath the western Yangtze block, South China: Evidence from whole-rock geochemistry and zircon U-Pb-Hf isotopes of mafic rocks", *Journal of Asian Earth Sciences*, vol. 206, p. 104616, 2021.

[61] L. Du, J. Guo, A. P. Nutman, et al., "Implications for rodinia reconstructions for the initiation of neoproterozoic subduction at ~860ma on the western margin of the Yangtze block: Evidence from the guandaoshan pluton", *Lithos*, vol. 196–197, pp. 67–82, 2014.

[62] Y. Zhu, S. Lai, J. Qin, et al., "Petrogenesis and geodynamic implications of neoproterozoic gabbro-diorites, adakitic granites, and a-type granites in the southwestern margin of the Yangtze block, South China", *Journal of Asian Earth Sciences*, vol. 183, p. 103977, 2019.

[63] W.-H. Sun, M.-F. Zhou, J.-F. Gao, Y.-H. Yang, X.-F. Zhao, and J.-H. Zhao, "Detrital zircon U–Pb geochronological and Lu–Hf isotopic constraints on the precambrian magmatic and crustal evolution of the western Yangtze Block, SW China", *Precambrian Research*, vol. 172, no. 1–2, pp. 99–126, 2009.

[64] U. Bednarz and H. U. Schmincke, "Mass transfer during sub-seafloor alteration of the upper troodos crust (cyprus)", *Contributions to Mineralogy and Petrology*, vol. 102, no. 1, pp. 93–101, 1989.

[65] L. Gélinas, M. Mellinger, and P. Trudel, "Archean mafic metavolcanics from the Rouyn–Noranda district, abitibi greenstone belt, Quebec. 1. mobility of the major elements", *Canadian Journal of Earth Sciences*, vol. 19, no. 12, pp. 2258–2275, 1982.

[66] G. Thompson, "Metamorphic and hydrothermal processes: Basalt-seawater interactions", in Oceanic Basalt, P.A. Floyd, Ed., pp. 148–173, Springer, New York, 1991.

[67] P. A. Floyd and J. A. Winchester, "Magma type and tectonic setting discrimination using immobile elements", *Earth and Planetary Science Letters*, vol. 27, no. 2, pp. 211–218, 1975.

[68] A. Polat, R. Kerrich, and D. A. Wyman, "Geochemical diversity in oceanic komatiites and basalts from the late Archean Wawa Greenstone belts, superior province, Canada: Trace element and Nd isotope evidence for a heterogeneous mantle", *Precambrian Research*, vol. 94, no. 3–4, pp. 139–173, 1999.

[69] A. D. Saunders, M. J. Norry, and J. Tarney, "Origin of MORB and chemically-depleted mantle reservoirs: Trace element constraints", *Journal of Petrology*, vol. Special_Volume, no. 1, pp. 415–445, 1988.

[70] J. Dostal, D. F. Strong, and R. A. Jamieson, "Trace element mobility in the mylonite zone within the ophiolite aureole, st. Anthony complex, Newfoundland", *Earth and Planetary Science Letters*, vol. 49, no. 2, pp. 188–192, 1980.

[71] J. J. Cramer and H. W. Nesbitt, "Mass balance relations and trace element mobility during continental weathering of various igneous rocks", *Sciences Géologiques, Bulletins et Mémoires*, vol. 73, pp. 63–73, 1983.

[72] L. L. Summa and K. L. Verosub, "Trace element mobility during early diagenesis of volcanic ash: Applications to stratigraphic correlation", *Quaternary International*, vol. 13–14, pp. 149–157, 1992.

[73] M. W. Schmidt and O. Jagoutz, "The global systematics of primitive arc melts", *Geochemistry, Geophysics, Geosystems*, vol. 18, no. 8, pp. 2817–2854, 2017.

[74] F. Jourdan, H. Bertrand, U. Schärer, J. Blichert-Toft, G. Féraud, and A. B. Kampunzu, "Major and trace element and Sr, Nd, Hf, and Pb isotope compositions of the karoo large igneous province, Botswana–Zimbabwe: Lithosphere vs mantle plume contribution", *Journal of Petrology*, vol. 48, no. 6, pp. 1043–1077, 2007.

[75] I. Y. Safonova, V. A. Simonov, E. V. Kurganskaya, O. T. Obut, R. L. Romer, and R. Seltmann, "Late paleozoic oceanic basalts hosted by the char suture-shear zone, East Kazakhstan: Geological position, geochemistry, petrogenesis and

tectonic setting", *Journal of Asian Earth Sciences*, vol. 49, pp. 20–39, 2012.

[76] I. Safonova, S. Kojima, S. Nakae, et al., "Oceanic island basalts in accretionary complexes of SW Japan: Tectonic and petrogenetic implications", *Journal of Asian Earth Sciences*, vol. 113, pp. 508–523, 2015.

[77] F. Albarède, Introduction to geochemical modelling, Cambridge University Press, Cambridge, 1995.

[78] J. H. Bédard, "Parental magmas of the nain plutonic suite anorthosites and mafic cumulates: A trace element modelling approach", *Contributions to Mineralogy and Petrology*, vol. 141, no. 6, pp. 747–771, 2001.

[79] S. Fretzdorff, R. A. Livermore, C. W. Devey, P. T. Leat, and P. Stoffers, "Petrogenesis of the back-arc East Scotia ridge, South Atlantic ocean", *Journal of Petrology*, vol. 43, no. 8, pp. 1435–1467, 2002.

[80] T. J. R. Ciborowski, A. C. Kerr, I. McDonald, R. E. Ernst, H. S. R. Hughes, and M. J. Minifie, "The geochemistry and petrogenesis of the paleoproterozoic Du chef dyke swarm, Québec, Canada", *Precambrian Research*, vol. 250, pp. 151–166, 2014.

[81] O. M. Turkina, A. E. Izokh, A. V. Lavrenchuk, and Ya. Yu. Shelepov, "Composition and isotope parameters of metabasalts and gabbroids of the onot granite–greenstone block, southwestern Siberian platform, as indicators of lithospheric mantle evolution from the archean to paleoproterozoic", *Petrology*, vol. 30, no. 5, pp. 499–522, 2022.

[82] H. Yang, P. Wu, A. Liu, and F. Wang, "Petrogenesis of the eocene highly fractionated granite porphyry with REE tetrad effect: An example from western Yunnan, southeastern Tibetan plateau", *Minerals*, vol. 13, no. 11, p. 1390, 2023.

[83] J. A. Pearce, I. J. Parkinson, et al, "Trace element models for mantle melting: Application to volcanic arc peterogenesis", in Magmatic processes and plate tectonics, H.M. Prichard, T. Alabaster, and N.B.W. Harris, Eds., 76:pp. 373–403, Geological Society of London, Special Publication, 1993.

[84] R. Kerrich and D. A. Wyman, "Review of developments in trace-element fingerprinting of geodynamic settings and their implications for mineral exploration", *Australian Journal of Earth Sciences*, vol. 44, no. 4, pp. 465–487, 1997.

[85] E. A. Codillo, V. Le Roux, and H. R. Marschall, "Arc-like magmas generated by mélange-peridotite interaction in the mantle wedge", *Nature Communications*, vol. 9, no. 1, 2018.

[86] R. P. Rapp, N. Shimizu, M. D. Norman, and G. S. Applegate, "Reaction between slab-derived melts and peridotite in the mantle wedge: Experimental constraints at 3.8 GPA", *Chemical Geology*, vol. 160, no. 4, pp. 335–356, 1999.

[87] J. C. Ayers, S. K. Dittmer, and G. D. Layne, "Partitioning of elements between peridotite and H_2O at 2.0–3.0 GPA and 900–1100°c, and application to models of subduction zone processes", *Earth and Planetary Science Letters*, vol. 150, no. 3–4, pp. 381–398, 1997.

[88] S. Skora and J. Blundy, "High-pressure hydrous phase relations of radiolarian clay and implications for the involvement of subducted sediment in arc magmatism", *Journal of Petrology*, vol. 51, no. 11, pp. 2211–2243, 2010.

[89] S. -S. Sun and W. F. McDonough, "Chemical and isotopic systematics of oceanic basalts: Implications for mantle composition and processes", *Geological Society, London, Special Publications*, vol. 42, no. 1, pp. 313–345, 1989.

[90] A. W. Hofmann, "Mantle geochemistry: The message from oceanic volcanism", *Nature*, vol. 385, no. 6613, pp. 219–229, 1997.

[91] V. A. Simonov, A. V. Mikolaichuk, I. Yu. Safonova, A. V. Kotlyarov, and S. V. Kovyazin, "Late paleozoic–cenozoic intra-plate continental basaltic magmatism of the Tien-shan–Junggar Region in the SW Central Asian Orogenic belt", *Gondwana Research*, vol. 27, no. 4, pp. 1646–1666, 2015.

[92] I. Safonova, S. Maruyama, S. Kojima, T. Komiya, S. Krivonogov, and K. Koshida, "Recognizing OIB and MORB in accretionary complexes: A new approach based on ocean plate stratigraphy, petrology and geochemistry", *Gondwana Research*, vol. 33, pp. 92–114, 2016.

[93] Y. Zhu, S. Lai, and W. Xie, "Wet calc-alkaline magmatic fractionation in the middle-upper crustal sections of the continental arc: Insights from the neoproterozoic nanba intrusive complex, western Yangtze block, South China", *Geological Society of America Bulletin*, vol. 136, no. 3–4, pp. 928–948, 2024.

[94] W. H. Sun and M. F. Zhou, "The 860-ma, cordilleran-type guandaoshan dioritic pluton in the Yangtze Block, SW China: Implications for the origin of neoproterozoic magmatism", *The Journal of Geology*, vol. 116, no. 3, pp. 238–253, 2008.

[95] M. Munteanu, A. Wilson, Y. Yao, C. Harris, G. Chunnett, and Y. Luo, "The tongde dioritic pluton (Sichuan, SW China) and its geotectonic setting: Regional implications of a local-scale study", *Gondwana Research*, vol. 18, no. 2–3, pp. 455–465, 2010.

[96] Z. X. Li, M. Cho, and X. H. Li, "Precambrian tectonics of East Asia and relevance to supercontinent evolution", *Precambrian Research*, vol. 122, no. 1–4, pp. 1–6, 2003.

[97] W. L. Ling, S. Gao, and B. R. Zhang, "Neoproterozoic tectonic evolution of the northwestern Yangtze craton, South China: Implications for amalgamation and break-up of the Rodinia supercontinent", *Precambrian Research*, vol. 122, no. 1–4, pp. 111–140, 2003.

[98] Z. Li, X. Li, W. Li, and S. Ding, "Was cathaysia part of proterozoic laurentia? – new data from Hainan island, South China", *Terra Nova*, vol. 20, no. 2, pp. 154–164, 2008.

[99] X.-H. Li, W.-X. Li, Z.-X. Li, et al., "Amalgamation between the Yangtze and Cathaysia blocks in South China: Constraints from SHRIMP U–Pb zircon ages, geochemistry and Nd–Hf isotopes of the Shuangxiwu volcanic rocks", *Precambrian Research*, vol. 174, no. 1–2, pp. 117–128, 2009.

[100] Z. X. Li, L. H. Zhang, and C. M. Powell, "South China in Rodinia: Part of the missing link between Australia–East Antarctica and Laurentia?", *Geology*, vol. 23, no. 5, 1995.

[101] W. Wang, M.-F. Zhou, D.-P. Yan, L. Li, and J. Malpas, "Detrital zircon record of neoproterozoic active-margin sedimentation in the eastern Jiangnan Orogen, South China", *Precambrian Research*, vol. 235, pp. 1–19, 2013.

[102] J. Yao, L. Shu, M. Santosh, and G. Zhao, "Neoproterozoic arc-related mafic–ultramafic rocks and syn-collision granite from the western segment of the Jiangnan Orogen, South China: Constraints on the neoproterozoic assembly of the Yangtze and Cathaysia Blocks", *Precambrian Research*, vol. 243, pp. 39–62, 2014.

[103] J.-H. Zhao, M.-F. Zhou, D.-P. Yan, J.-P. Zheng, and J.-W. Li, "Reappraisal of the ages of neoproterozoic strata in South

China: No connection with the grenvillian orogeny", *Geology*, vol. 39, no. 4, pp. 299–302, 2011.

[104] X. Wang, J. Zhou, J. Qiu, and J. Gao, "Geochemistry of the meso- to neoproterozoic basic–acid rocks from Hunan province, South China: Implications for the evolution of the western Jiangnan Orogen", *Precambrian Research*, vol. 135, no. 1–2, pp. 79–103, 2004.

[105] X.-L. Wang, J.-C. Zhou, W. L. Griffin, et al., "Geochemical zonation across a neoproterozoic orogenic belt: Isotopic evidence from granitoids and metasedimentary rocks of the Jiangnan Orogen, China", *Precambrian Research*, vol. 242, pp. 154–171, 2014.

[106] L. Li, S. Lin, G. Xing, et al., "Geochronology and geochemistry of volcanic rocks from the shaojiwa formation and xingzi group, Lushan Area, SE China: Implications for neoproterozoic back-arc basin in the Yangtze Block", *Precambrian Research*, vol. 238, pp. 1–17, 2013.

[107] R. E. Ernst, K. L. Buchan, and I. H. Campbell, "Frontiers in large igneous province research", *Lithos*, vol. 79, no. 3–4, pp. 271–297, 2005.

[108] M. K. Reichow, M. S. Pringle, A. I. Al'Mukhamedov, et al., "The timing and extent of the eruption of the Siberian traps large igneous province: Implications for the end-permian environmental crisis", *Earth and Planetary Science Letters*, vol. 277, no. 1–2, pp. 9–20, 2009.

[109] S. E. Bryan and L. Ferrari, "Large igneous provinces and silicic large igneous provinces: Progress in our understanding over the last 25 years", *Geological Society of America Bulletin*, vol. 125, no. 7–8, pp. 1053–1078, 2013.

[110] J. G. Shellnutt, "The emeishan large igneous province: A synthesis", *Geoscience Frontiers*, vol. 5, no. 3, pp. 369–394, 2014.

[111] M. M. Buslov, I. Yu. Safonova, G. S. Fedoseev, M. K. Reichow, K. Davies, and G. A. Babin, "Permo-triassic plume magmatism of the Kuznetsk Basin, Central Asia: Geology, geochronology, and geochemistry", *Russian Geology and Geophysics*, vol. 51, no. 9, pp. 1021–1036, 2010.

[112] A. A. P. Koppers, T. W. Becker, M. G. Jackson, et al., "Mantle plumes and their role in earth processes", *Nature Reviews Earth & Environment*, vol. 2, no. 6, pp. 382–401, 2021.

[113] M.-F. Zhou, D.-P. Yan, A. K. Kennedy, Y. Li, and J. Ding, "SHRIMP U–Pb zircon geochronological and geochemical evidence for neoproterozoic arc-magmatism along the western margin of the Yangtze block, South China", *Earth and Planetary Science Letters*, vol. 196, no. 1–2, pp. 51–67, 2002.

[114] M.-F. Zhou, D.-P. Yan, C.-L. Wang, L. Qi, and A. Kennedy, "Subduction-related origin of the 750 ma xuelongbao adakitic complex (Sichuan province, China): Implications for the tectonic setting of the giant neoproterozoic magmatic event in South China", *Earth and Planetary Science Letters*, vol. 248, no. 1–2, pp. 286–300, 2006.

[115] X.-L. Huang, Y.-G. Xu, J.-B. Lan, Q.-J. Yang, and Z.-Y. Luo, "Neoproterozoic adakitic rocks from mopanshan in the western Yangtze craton: Partial melts of a thickened lower crust", *Lithos*, vol. 112, no. 3–4, pp. 367–381, 2009.

[116] W. Wang, S. Liu, Y. Feng, et al., "Chronology, petrogenesis and tectonic setting of the neoproterozoic tongchang dioritic pluton at the northwestern margin of the Yangtze Block: Constraints from geochemistry and zircon U–Pb–Hf isotopic systematics", *Gondwana Research*, vol. 22, no. 2, pp. 699–716, 2012.

[117] W.-G. Zhu, H. Zhong, X.-H. Li, et al., "SHRIMP zircon U–Pb geochronology, elemental, and Nd isotopic geochemistry of the neoproterozoic mafic dykes in the Yanbian area, SW China", *Precambrian Research*, vol. 164, no. 1–2, pp. 66–85, 2008.

[118] X. Cui, X. Jiang, J. Wang, et al., "Mid-neoproterozoic diabase dykes from xide in the western Yangtze Block, South China: New evidence for continental rifting related to the breakup of Rodinia supercontinent", *Precambrian Research*, vol. 268, pp. 339–356, 2015.

[119] H. Li, Z. Zhang, M. Santosh, et al., "Geochronological, geochemical and Sr–Nd isotopic fingerprinting of neoproterozoic mafic dykes in the western margin of the Yangtze Block, SW China: Implications for Rodinia supercontinent breakup", *Precambrian Research*, vol. 331, 2019.

[120] P. Druschke, A. D. Hanson, Q. Yan, Z. Wang, and T. Wang, "Stratigraphic and U-Pb SHRIMP detrital zircon evidence for a neoproterozoic continental arc, Central China: Rodinia implications", *The Journal of Geology*, vol. 114, no. 5, pp. 627–636, 2006.

[121] P. A. Cawood, Y. Wang, Y. Xu, and G. Zhao, "Locating South China in Rodinia and Gondwana: A fragment of greater India lithosphere?", *Geology*, vol. 41, no. 8, pp. 903–906, 2013.

[122] X. H. Li, H. W. Zhou, Z. X. Li, et al, "Zircon U-Pb age and petrochemical characteristics of the neoproterozoic bimodal volcanics from western Yangtze Block(In Chinese)", Geochimica, vol. 30, no. 4, pp. 315–322, 2001.

[123] B. Hui, Y. Dong, G. Liu, et al., "Origin of mafic intrusions in the Micangshan massif, Central China: Implications for the neoproterozoic tectonic evolution of the northwestern Yangtze Block", *Journal of Asian Earth Sciences*, vol. 190, p. 104132, 2020.

[124] Y. Dong, B. Hui, S. Sun, et al., "Neoproterozoic tectonic evolution and proto-Basin of the Yangtze Block, China", *Earth-Science Reviews*, vol. 249, p. 104669, 2024.

[125] H. Shinjoe, "Origin of the granodiorite in the forearc region of Southwest Japan: Melting of the shimanto accretionary prism", *Chemical Geology*, vol. 134, no. 4, pp. 237–255, 1997.

[126] R. Shinjo, "Geochemistry of high Mg andesites and the tectonic evolution of the okinawa trough–ryukyu arc system", *Chemical Geology*, vol. 157, no. 1–2, pp. 69–88, 1999.

[127] O. Okano, T. Sato, and H. Kagami, "Rb–Sr and Sm–Nd isotopic studies of mafic igneous rocks from the ryoke plutono-metamorphic belt in the Setouchi area, Southwest Japan: Implications for the genesis and thermal history", *Island Arc*, vol. 9, no. 1, pp. 21–36, 2000.

[128] B. M. Jahn, "Accretionary Orogen and evolution of the Japanese islands: Implications from a Sr-Nd isotopic study of the phanerozoic granitoids from SW Japan", *American Journal of Science*, vol. 310, no. 10, pp. 1210–1249, 2010.

[129] I. Kita, Y. Asakawa, T. Yuri, et al., "Rifting of Kyushu, Japan, based on the fault-controlled concurrent eruption of oceanic island basalt-type and island arc-type lavas", *Bulletin of Volcanology*, vol. 74, no. 5, pp. 1121–1139, 2012.

[130] J. Kimura, J. B. Gill, T. Kunikiyo, et al, "Diverse magmatic effects of subducting a hot slab in SW Japan: Results from

forward modeling", *Geochemistry, Geophysics, Geosystems*, vol. 15, no. 3, pp. 691–739, 2014.

[131] E. Akasaki, M. Owada, and A. Kamei, "Crustal differentiation due to partial melting of granitic rocks in an active continental margin, the Ryoke Belt, southwest Japan", *Lithos*, vol. 230, pp. 82–91, 2015.

[132] X.-F. Zhao, M.-F. Zhou, J.-W. Li, and F.-Y. Wu, "Association of neoproterozoic a- and i-type granites in South China: Implications for generation of a-type granites in a subduction-related environment", *Chemical Geology*, vol. 257, no. 1–2, pp. 1–15, 2008.

[133] E. A. K. Middlemost, "Naming materials in the magma/igneous rock system", *Earth-Science Reviews*, vol. 37, no. 3–4, pp. 215–224, 1994.

[134] J. A. Winchester and P. A. Floyd, "Geochemical discrimination of different magma series and their differentiation products using immobile elements", *Chemical Geology*, vol. 20, pp. 325–343, 1977.

[135] T. N. Irvine and W. R. A. Baragar, "A guide to the chemical classification of the common volcanic rocks", *Canadian Journal of Earth Sciences*, vol. 8, no. 5, pp. 523–548, 1971.

[136] A. Peccerillo and S. R. Taylor, "Geochemistry of eocene calc-alkaline volcanic rocks from the Kastamonu area, northern Turkey", *Contributions to Mineralogy and Petrology*, vol. 58, no. 1, pp. 63–81, 1976.

[137] C. B. Keller, B. Schoene, M. Barboni, K. M. Samperton, and J. M. Husson, "Volcanic-plutonic parity and the differentiation of the continental crust", *Nature*, vol. 523, no. 7560, pp. 301–307, 2015.

[138] T. Hanyu, Y. Tatsumi, S. Nakai, et al., "Contribution of slab melting and slab dehydration to magmatism in the NE Japan arc for the last 25 myr: Constraints from geochemistry", *Geochemistry, Geophysics, Geosystems*, vol. 7, no. 8, p. 8, 2006.

[139] J. D. Vervoort, P. J. Patchett, J. Blichert-Toft, and F. Albarède, "Relationships between Lu–Hf and Sm–Nd isotopic systems in the global sedimentary system", *Earth and Planetary Science Letters*, vol. 168, no. 1–2, pp. 79–99, 1999.

[140] Y. Zhu, S. Lai, W. Xie, et al., "Neoproterozoic tectonic transition from subduction to back-arc extension along the western Yangtze Block, South China: Petrological evidence of Nb-enriched basalts and arc-type intrusive rocks", *Gondwana Research*, vol. 122, pp. 163–180, 2023.

[141] T. Plank and C. H. Langmuir, "The chemical composition of subducting sediment and its consequences for the crust and mantle", *Chemical Geology*, vol. 145, no. 3–4, pp. 325–394, 1998.

[142] K. T. M. Johnson, "Experimental determination of partition coefficients for rare earth and high-field-strength elements between clinopyroxene, garnet, and basaltic melt at high pressures", *Contributions to Mineralogy and Petrology*, vol. 133, no. 1–2, pp. 60–68, 1998.

[143] L. P. Bedard, "Graphical comparison of geochemical results", *Geostandards Newsletter*, vol. 18, no. 1, pp. 101–103, 1994.

[144] I. Safonova, G. Biske, R. L. Romer, R. Seltmann, V. Simonov, and S. Maruyama, "Middle paleozoic mafic magmatism and ocean plate stratigraphy of the South Tianshan, Kyrgyzstan", *Gondwana Research*, vol. 30, pp. 236–256, 2016.

[145] D. A. Wood, "The application of a thhfta diagram to problems of tectonomagmatic classification and to establishing the nature of crustal contamination of basaltic lavas of the british tertiary volcanic province", *Earth and Planetary Science Letters*, vol. 50, no. 1, pp. 11–30, 1980.

[146] B. Cabanis and M. Lecolle, "Le diagramme la/10-y/15-nb/8: Un_outil pour la discrimination des series volcaniques et la mise en evidence des processus de melande et/ou de contamination crustale", *Comptes Rendus de l'Académie Des Sciences. Série*, vol. 309, pp. 2023–2029, 1989.

[147] M. Meschede, "A method of discriminating between different types of mid-ocean ridge basalts and continental tholeiites with the Nb-Zr-Y diagram", *Chemical Geology*, vol. 56, no. 3–4, pp. 207–218, 1986.

[148] J. A. Pearce, "Geochemical fingerprinting of oceanic basalts with applications to ophiolite classification and the search for archean oceanic crust", *Lithos*, vol. 100, no. 1–4, pp. 14–48, 2008.

[149] H. Kagami, S. Iizumi, Y. Tainosho, and M. Owada, "Spatial variations of Sr and Nd isotope ratios of cretaceous-paleogene granitoid rocks, Southwest Japan arc", *Contributions to Mineralogy and Petrology*, vol. 112, no. 2–3, pp. 165–177, 1992.

[150] M. Yuhara, H. Kagami, and K. Nagao, "Geochronological characterization and petrogenesis of granitoids in the Ryoke Belt, Southwest Japan arc: Constraints from K–Ar, Rb–Sr and Sm-Nd systematics", *Island Arc*, vol. 9, no. 1, pp. 64–80, 2000.

[151] J. I. Kimura and T. Yoshida, "Contributions of slab fluid, mantle wedge and crust to the origin of quaternary lavas in the NE Japan arc", *Journal of Petrology*, vol. 47, no. 11, pp. 2185–2232, 2006.

[152] T. Shibata, M. Yoshikawa, J. Itoh, O. Ujike, M. Miyoshi, and K. Takemura, "Along-arc geochemical variations in quaternary magmas of northern Kyushu island, Japan", *Geological Society, London, Special Publications*, vol. 385, no. 1, pp. 15–29, 2014.

[153] G. Zhao, W. Luo, Z. Lai, L. Tian, and C. Xu, "Influence of subduction components on magma composition in back-arc basins: A comparison between the Mariana and Okinawa troughs", *Geological Journal*, vol. 51, no. S1, pp. 357–367, 2016.

[154] Y. Shu, S. G. Nielsen, Z. Zeng, et al., "Tracing subducted sediment inputs to the Ryukyu arc-okinawa trough system: Evidence from thallium isotopes", *Geochimica et Cosmochimica Acta*, vol. 217, pp. 462–491, 2017.

[155] Y. Zhang, Y. Shu, S. Turner, Z. Chen, Z. Zeng, and F. Huang, "Deciphering contribution of recycled altered oceanic crust to arc magmas using Ba-Sr-Nd isotopes", *Journal of Geophysical Research*, vol. 129, no. 3, 2024.